

RESEARCH ARTICLE

Modulation of signaling cross-talk between pJNK and pAKT generates optimal apoptotic response

Sharmila Biswas¹ , Baishakhi Tikader² , Sandip Kar^{2*}, Ganesh A. Viswanathan^{1*} 

1 Department of Chemical Engineering, Indian Institute of Technology Bombay, Mumbai, India,

2 Department of Chemistry, Indian Institute of Technology Bombay, Mumbai, India

 These authors contributed equally to this work.

* sandipkar@iitb.ac.in (SK); ganeshav@iitb.ac.in (GAV)



Abstract

Tumor necrosis factor alpha (TNF α) is a well-known modulator of apoptosis by maintaining a balance between proliferation and cell-death in normal cells. Cancer cells often evade apoptotic response following TNF α stimulation by altering signaling cross-talks. Thus, varying the extent of signaling cross-talk could enable optimal TNF α mediated apoptotic dynamics. Herein, we use an experimental data-driven mathematical modeling to quantitate the extent of synergistic signaling cross-talk between the intracellular entities phosphorylated JNK (pJNK) and phosphorylated AKT (pAKT) that orchestrate the phenotypic apoptosis level by modulating the activated Caspase3 dynamics. Our study reveals that this modulation is orchestrated by the distinct dynamic nature of the synergism at early and late phases. We show that this synergism in signal flow is governed by branches originating from either TNF α receptor and NF κ B, which facilitates signaling through survival pathways. We demonstrate that the experimentally quantified apoptosis levels semi-quantitatively correlates with the model simulated Caspase3 transients. Interestingly, perturbing pJNK and pAKT transient dynamics fine-tunes this accumulated Caspase3 guided apoptotic response. Thus, our study offers useful insights for identifying potential targeted therapies for optimal apoptotic response.

OPEN ACCESS

Citation: Biswas S, Tikader B, Kar S, Viswanathan GA (2022) Modulation of signaling cross-talk between pJNK and pAKT generates optimal apoptotic response. *PLoS Comput Biol* 18(10): e1010626. <https://doi.org/10.1371/journal.pcbi.1010626>

Editor: Jing Chen, Virginia Polytechnic Institute and State University, UNITED STATES

Received: May 23, 2022

Accepted: October 3, 2022

Published: October 14, 2022

Peer Review History: PLOS recognizes the benefits of transparency in the peer review process; therefore, we enable the publication of all of the content of peer review and author responses alongside final, published articles. The editorial history of this article is available here: <https://doi.org/10.1371/journal.pcbi.1010626>

Copyright: © 2022 Biswas et al. This is an open access article distributed under the terms of the [Creative Commons Attribution License](https://creativecommons.org/licenses/by/4.0/), which permits unrestricted use, distribution, and reproduction in any medium, provided the original author and source are credited.

Data Availability Statement: All data are in the manuscript and/or [supporting information files](#). The GitHub repository at <https://github.com/baichat90/SB-BT-Modulation-of-TNF-mediated->

Author summary

TNF α mediated apoptosis, a form of cell-death, is the desired outcome for cancer therapeutics. This outcome is governed by complex regulation involving several signaling entities stimulated by TNF α . Relating the transient levels of these entities over early phase of the signaling response to the late-phase cell-death is a challenge. We developed a knowledge and data-driven mathematical model to unravel the dynamic synergistic correlation between the early transients governing the apoptotic response. Using flux balance and branch analysis, we demonstrated that the dynamic cross-talk between different key signaling entities regulates the apoptotic response. We performed inhibitory experiments predicted by model simulations and thereby established that cells tweak the extent of

[crosstalk-06092022](#) contains the raw experimental data, the codes for parameter estimation and model analysis, and ReadMe file.

Funding: This study was funded by the grants CRG/2020/002672 (GAV), MTR/2020/000589 (GAV), CRG/2019/002640 (SK), and MTR/2020/000261 (SK) from Science and Engineering Research Board (SERB India; <http://www.serb.gov.in>), Department of Science and Technology, Government of India. The funders had no role in study design, data collection and analysis, decision to publish, or preparation of the manuscript.

Competing interests: The authors have declared that no competing interests exist.

synergism during signal transduction to modulate the apoptotic response in a time-dependent manner. Thus, our approach provides useful insights for identifying signaling targets to arrive at novel combinatorial cancer therapies.

Introduction

The pleiotropic cytokine Tumor necrosis factor alpha (TNF α) mediates diverse cellular phenotypic decisions such as apoptosis, inflammation, proliferation [1–9]. In normal cells, TNF α maintains a balance between different phenotypes [10]. Since such a balance is disrupted in a diseased cell in a cancer or autoimmune milieu [11–14], its restoration using interventional therapeutic approach involving TNF α is being considered recently [15,16]. Often these strategies become ineffective to cause optimal apoptosis [17,18]. This is because TNF α activates a number of signaling pathways [19,20] culminating in varied apoptotic response. This leads to a question as how to optimally control the TNF α mediated apoptotic dynamics in a cell-type specific manner.

One of the primary events involved in cells exhibiting an apoptotic response is activation of Caspase3. Caspase3 is one of the effector caspases and is a key player involved in regulation of cell-death [11,19,21,22]. Along with modulating cell-death, TNF α strongly controls the survival responses by transducing information through entities such as NF κ B [21,23–26], pAKT which is activated by PI3K [27–30]. These entities along with pJNK are well-known regulators of survival and apoptosis [31,32]. However, the extent of dynamic signaling cross-talk between these entities regulating the optimal cell-type specific apoptotic outcome remains unclear.

Mathematical modeling of molecular network [33–35] that regulates a cell's response to TNF α enables quantification of the dynamic behavior of various entities [2,36]. These network modeling frameworks provide an opportunity to investigate underlying signaling cross-talk behavior in a context-specific manner. For example, a combined computational and perturbative experimental study showed that along with other intracellular phospho-proteins, pAKT may be involved in influencing the stimulus-strength dependent kinetics of the short-term (4 h) TNF α signaling induced apoptotic response [37,38]. These studies suggest that in shorter time scales, pAKT could be a key modulator of TNF α induced apoptosis via Caspase3 activation. However, apoptosis in mammalian systems occurs over much larger timescales. Correlating these observations across timescales requires a detailed investigation of the TNF α triggered activation of Caspase3, whose early phase transients are regulated by various intracellular proteins, among which a key regulator is NF κ B [39].

NF κ B transients in a cell stimulated by TNF α contain sufficient information to sense the stimulus dose and accordingly fine-tune the regulation of cellular responses [40]. Recent study on NIH3T3 cells demonstrated that NF κ B dynamics precisely reflects the rate of change in dose of TNF α stimulation [41]. The underlying TNF α molecular network contains several integrated pathways and multiple feedback regulations. Both quantitative and qualitative mathematical models of the network could provide a precise understanding of the dynamical properties of such a complex system. Single-cell level model of the TNF α dose-dependent NF κ B signaling revealed that a cell's commitment to apoptotic or proliferative phenotype could be embedded in the early transient response of NF κ B [42]. This raises a question as to how precisely the early NF κ B transients refine the sustained Caspase3 activation that eventually results in a long-term apoptotic response.

Discrete-level models of TNF α network predicted the experimentally observed qualitative trend of phenotypic pro-survival and apoptotic response [43,44]. While discrete-level

modelling offers identification of signaling trends, it cannot account for time-dependent correlations which is required for unravelling the extent of cross-talk between different entities. However, predicting dynamic cross-talk and its ensuing effects on the long-term phenotypic response requires a detailed kinetic modelling. Recent kinetic modelling showed that TNF α mediated apoptosis is influenced by the TNF α level [45–47] and the overall mitochondrial mass [48]. These do not reveal the underlying dynamic signaling cross-talk between various intra-cellular intermediate entities.

Hence, the goal of this study is to decipher the dynamic signaling cross-talk between the key intracellular entities that regulates Caspase3 downstream and subsequently correlate it with the phenotypic apoptotic response. In order to achieve this objective, we took an experimental data-constrained systems biology approach. In particular, we seek to distill out this dynamic cross-talk regulating the TNF α mediated phenotypic apoptotic outcome in a context-dependent manner by considering U937 as a model cell line. The parameters involved in the kinetic model needs to be estimated, as these are not available in the literature for the considered cell-type. The methodology adopted leads to grossly identifiable sets of model parameters and thereby making our multi-input model predictive. We quantify the transient contributions by pJNK, pAKT and Caspase3, and their combinatorial effect that govern the hidden dynamic correlation using a detailed flux and branch analysis of the model of TNF α network. Our study revealed that targeted inhibitors can refine the dynamic cross-talk as well as the apoptotic outcome.

Results

NF κ B signal inhibition enhances TNF α mediated apoptotic response

To study the dynamics of cellular fate on soluble 17.3kDa TNF α stimulation, we measured the apoptosis fraction using Annexin V assay (Methods) in the U937 cells. A 24 h exposure of TNF α (100 ng/ml) results in 25% of the population undergoing cell-death (Fig 1A, blue bar) (Details of estimation of the cell-death along with associated controls are in S1 Text). Low cell-death following exposure to only TNF α indicates that in U937 cells the cytokine might be favoring the survival signaling as well [2] and maintains a balance between the apoptotic and survival responses. As a strong mediator of survival signaling [11], NF κ B is likely to be activated in response to TNF α stimulation in U937 cells. In order to ascertain its involvement, we exposed U937 cells to Triptolide (TPL) which blocks NF κ B transactivation and thereby arrested signal flow through survival pathways [49]. The relative drop in the survival response due to TPL confirms NF κ B inhibition in U937 cells (S1 Fig). Pre-treatment with TPL (60 nM) and subsequent exposure to TNF α resulted in 80% cell death (Fig 1A, black bar). A comparison of apoptosis levels for this case with those corresponding to only TPL (Fig 1A, red bar) pre-treatment determines that blocking survival pathway in U937 can lead to sufficient apoptotic response. However, those cells experiencing a pre-treatment of TPL showed a greater initial (8 h) apoptotic response in the presence of TNF α (Fig 1A, red and black bars). At the same time, the levels of cell death in the case of only TPL, and those pre-treated with TPL and exposed to TNF α were similar at 24h. This indicates that the survival signaling pathway coordinates with those of apoptosis in order to regulate the cell-death in U937 cells. Overall, in the early phase (<8 hours), the apoptosis level during the combined treatment is nearly equal to the sum of that achieved for individual TPL and TNF α stimulation hints the presence of a synergistic response. On the contrary, in the later phase (>8 hours), the apoptosis levels for TPL and TPL+TNF α treatment are nearly equal. However, these responses do not reveal how signal flow through different branches of the network orchestrates this synergism.

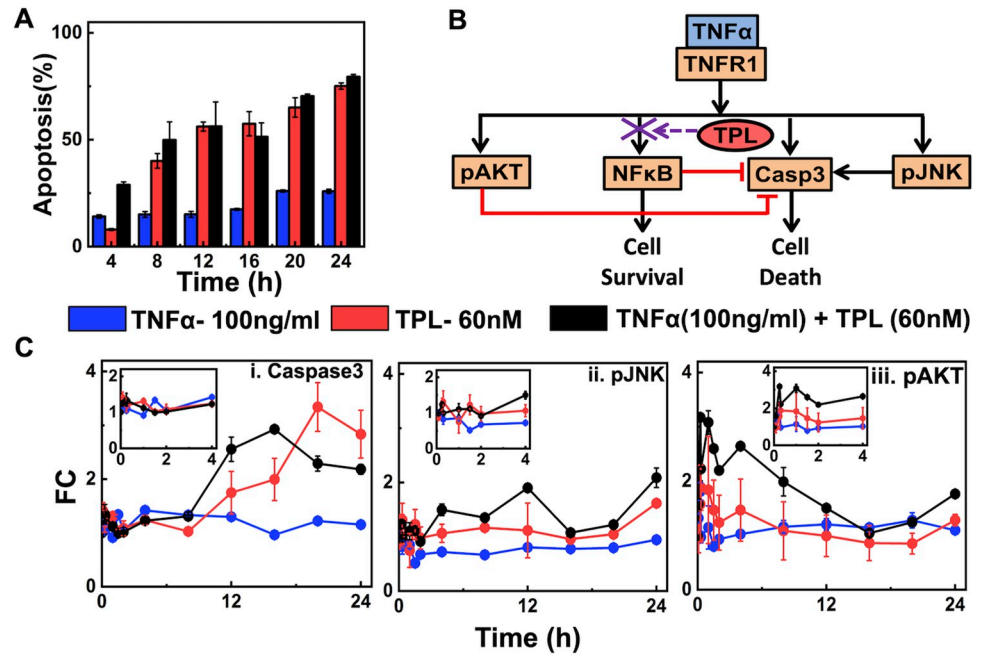


Fig 1. Apoptosis and intracellular signaling patterns due to TNF α stimulation in the presence and absence of NF κ B activity. (A) Cell death percentage measured using Annexin V assay under three different experimental conditions at different time points. (B) A schematic of TNF α signaling mediating survival and apoptotic responses via key intracellular regulators. (C) Trajectories of relative fold change (FC), as defined by Eq (4) in Methods, of (i) Caspase3, (ii) pJNK, and (iii) pAKT for three different experimental conditions (insets show the zoomed version for the first 4 hours). Experiments were done in triplicates using U937 cells. Details of extraction of apoptosis percentage along with controls of intracellular proteins, and trajectories of untreated cells over 24h time period are presented in [S1 Text](#).

<https://doi.org/10.1371/journal.pcbi.1010626.g001>

Deciphering this synergism requires distilling out the intracellular dynamic features that govern the survival and apoptotic responses in TNF α stimulated U937 cells. The key regulatory entities involved in this orchestration are depicted in [Fig 1B](#). It is well established that the two upstream signaling entities pAKT and pJNK regulate apoptosis [38,50,51]. pAKT has a significant role in preventing Caspase3 activation [52]. pJNK has a role in activating downstream caspases [53] and thereby regulating cellular apoptosis. This role of pJNK has been found to be context-specific [53,54]. Thus, we simultaneously measured the dynamic levels (in terms of relative fold change (FC)) of these activated signaling proteins using high-throughput experimentation [55,56] (Methods; [S1 Text](#)), which are presented in [Fig 1C](#). In the case of only TNF α stimulation, Caspase3 dynamics being relatively unaltered for the entire duration ([Fig 1Ci](#), blue) corroborates with the low apoptosis percentage over 24 hours ([Fig 1A](#), blue bar). Note that even for pJNK and pAKT trajectories for the case of only TNF α stimulation, an initial increase in the fold change was observed ([Fig 1Cii-1Ciii](#) (inset), blue bar). On the other hand, under NF κ B inhibitory conditions (TPL and TNF α + TPL), a rise in the later time period (>8h) of the Caspase3 FC ([Fig 1Ci](#), red and black bars) commensurate with the enhanced cell death as found in [Fig 1A](#) (red and black bars). The subsequent continuous decrease in pAKT is reflected by a sustained increase of Caspase3 levels.

These results suggest that cells undergo enhanced apoptosis as well as a marked change in the dynamics of pAKT, pJNK and Caspase3, if NF κ B mediated survival signaling is inhibited using TPL. However, the extent of dynamical crosstalk between these intracellular entities cannot be inferred from such observations. Therefore, how the dynamics of upstream proteins refine the downstream Caspase3 response, eventually regulating the apoptosis, cannot be

determined from these observations. It remains inconclusive as to which entities could be tuned to regulate the cellular decision-making events involved in cell survival or apoptosis. Moreover, the synergism in eliciting distinct apoptotic responses in the early and later phases cannot be identified using the simple network proposed in Fig 1B. Thus, to understand how the crosstalk between multiple intracellular dynamic signals quantitatively modulates cellular apoptosis, we need to develop a predictive mathematical model of the underlying TNF α network.

Data-driven mathematical model of TNF α network

The TNF α network wiring diagram considered for the data-driven mathematical model is depicted in Fig 2A, which is an expanded version of Fig 1B. Biochemical details of the interactions in Fig 2A are presented in S2 Text and S2 Fig. The network model (Fig 2A) assumes that soluble 17.3kDa TNF α upon binding to membrane bound TNFR1 activates MAPK cascades (pERK and pJNK), NF κ B and pAKT survival pathways along with the Caspase3 pathway, which mediates apoptosis [2]. (Since TNFR2 is activated only by 26kDa transmembrane TNF α , TNFR2 and its downstream signaling are excluded.) Molecular players such as ceramide are also activated upon TNF α stimulation, which subsequently influence the pAKT and pJNK levels [57]. MKK4/7, ROS and pJNK are involved in a positive feedback loop. As NF κ B inhibition resulted in an augmented level of apoptosis (Fig 1), we included nodes governed by NF κ B. These nodes are involved in activation or inhibition of pAKT, pJNK and Caspase3. In our model, Bcl2 and PI3K directly activate pAKT, while CAPP inhibits pAKT. TNFR1 and pJNK activate Caspase3, while pAKT and NF κ B inhibits Caspase3. MKK4/7 and C1P induce the activation of pJNK, but ERK1/2 and XIAP/Gadd45 β deactivate pJNK expression. We incorporated these entities into the model to extensively study the signaling cross-talk between these entities leading to apoptosis regulation [58–60]. To reduce the network complexity, we introduced direct or minimal set of interactions to account for long-range feedbacks. Interactions (Figs 2A and S2) represent either direct activation, direct inhibition or overall causal effect due to a complex set of sequential biological regulations. While some of these interactions were expressed in terms of mass-action kinetics, the remaining were modeled using either Michaelis-Menten or Hill-type kinetics to appropriately capture the underlying nonlinear behavior. (Details of each of these are given in Table I in S2 Text.)

The proposed mathematical kinetic model of the network (S1, S2 and S3 Tables) was calibrated using experimentally observed relative FC data of pJNK, pAKT and Caspase3. (Details of the calibration are given in S3 Fig) By implementing the appropriate statistical criteria (Methods; S2 Text), the kinetic parameters were estimated (S3 Table). Boxplot analysis revealed that the 3% best-fit parameter sets (out of 2000 samples) are reasonably identifiable (S4 Fig). These 3% parameter sets were used for generating model simulated trajectories, which fit well with the experimental data within the error margin, as shown in Fig 2B. (S5 Fig shows the best-fit trajectory.) Model simulations show that inhibition of NF κ B by TPL cannot be restored even in the presence of a combination of TPL and TNF α (S3 Text and S6 and S7 Figs) which substantiates the similarity in the transient Caspase3 dynamics for TPL and TNF α +TPL treatments (Fig 2Bvi and 2Bix). This further shows that TPL inhibition is indeed significant in shutting down the activity of NF κ B.

In order to test the predictive ability of the model, we examined the simulated transients with independent experimental observations obtained for cells pre-treated with lower concentration of TPL (10 nM) in the presence TNF α (S8 Fig). The small mean square displacements between the experimental data and simulated trajectories indicate that the model predicted pAKT, JNK and Caspase3 dynamics with reasonable accuracy (S8 Fig). Moreover, under TPL

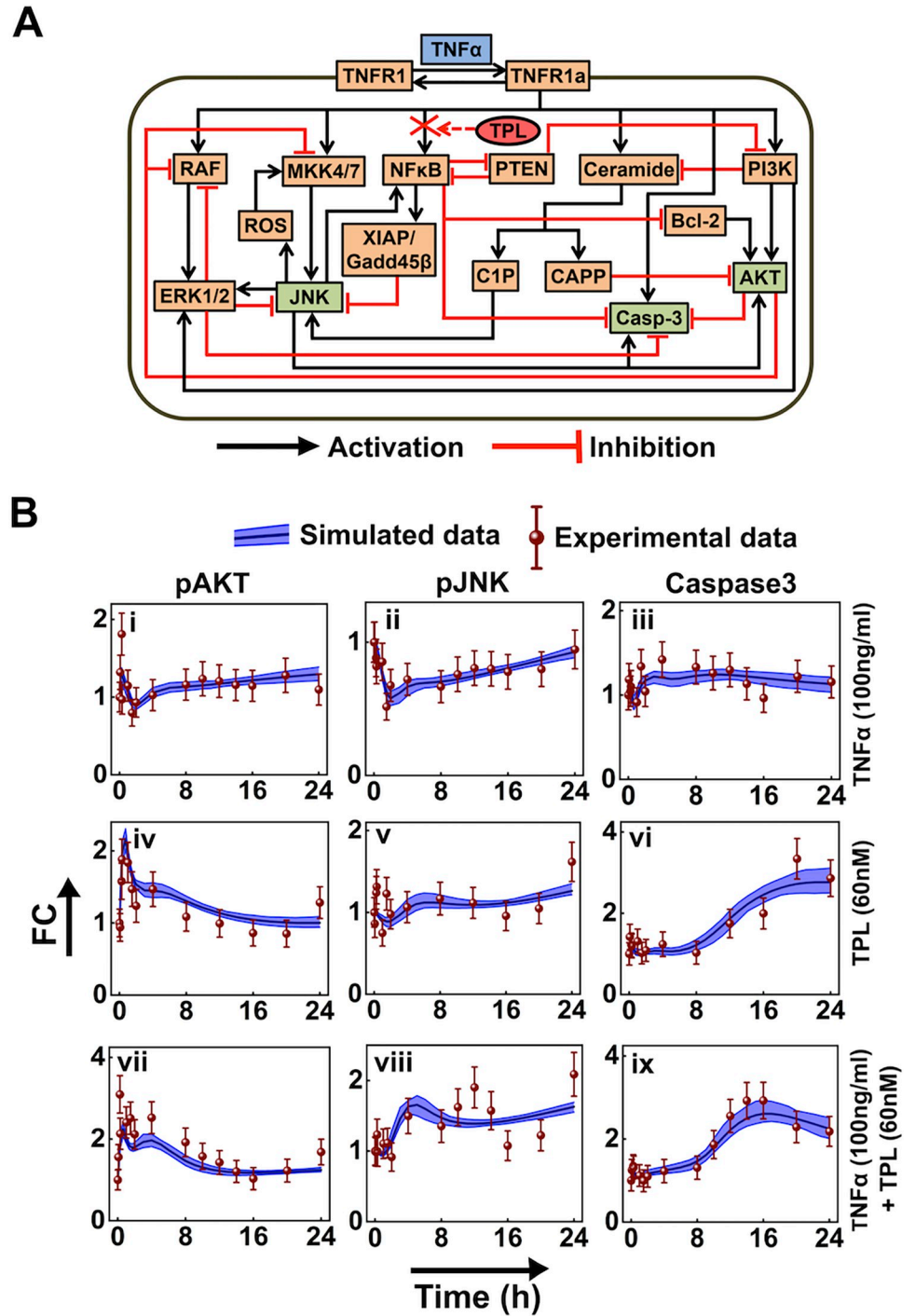


Fig 2. Interaction network and model training with quantitative time resolved data of U937 cells. (A) Schematic of TNF α signaling network. Black arrows and red hammers, respectively represent activation and inhibition of entities. While green boxes indicate experimentally measured marker proteins, red cross captures NF κ B inhibition by TPL (red oval). Multiple pathways from NF κ B inhibiting Caspase3 are lumped as a single inhibitory interaction. (Details of the entities and the interactions are in S2 Text.) (B) A comparison of the experimentally measured (red-wine circles) and model estimated signaling marker trajectory of pAKT (i, iv, vii), pJNK (ii, v, viii), and Caspase3 (iii, vi, ix) under different stimulation conditions. In each of these, black lines capture the mean of best 3% model-fitted trajectories. The blue cloud around the mean encompasses all 3% best-fitted trajectories. Note that the experimental measurements are those in Fig 1C. To constrain the model better, two additional data points (10 and 14 hours) were included during parameter estimation. The levels at these two time points were estimated using spline fitting the experimental data. Error bar around each experimental data point were calculated using standard error model.

<https://doi.org/10.1371/journal.pcbi.1010626.g002>

(10 nM)+TNF α (100 ng/ml) case, analysis of the relative influence of identified cross-talk related parameters on the predicted dynamics of these entities revealed that the pAKT and pJNK dynamics are the least sensitive (S9 Fig). On the other hand, the Caspase3 dynamics is sensitive to some of the parameters to a higher extent (S9 Fig).

Overall, the mathematical model of the network reliably mimics our experimental findings. However, mere comparison of the transients of the marker proteins do not offer insights into how the overall dynamics is regulated. Such an insight can be obtained by systematically unraveling the dynamic cross-talk between various entities. Unless otherwise stated explicitly, we will use the model with the identified best parameter sets for further cross-talk analysis.

Unraveling the dynamic cross-talk between signaling entities in the network

We next focus on unraveling the dynamic cross-talk between pAKT, pJNK and Caspase3 transients. We quantitate this by analyzing influence of specific entities in the network (Fig 2A) on these transients by capturing the corresponding biochemical reaction rate or flux. A signal flowing via an interaction from a start to an end node can be quantified by the reaction flux transduced by it. This reaction flux via an interaction is specified by the rate at which the start node influences the dynamics of the end node. Note that the instantaneous level of a certain protein is a linear combination of the contributing fluxes with appropriate sign. (Details of flux calculations along with associated expressions are provided in S4 Text.) We track the dynamic evolution of these fluxes (S10 Fig) under all three stimulation conditions (TNF α , TPL, TNF α + TPL). We present in Fig 3 the dynamic evolution of the fluxes of the interactions that contribute significantly to the transient levels of pAKT, pJNK and Caspase3.

The reaction flux analysis shows that pAKT dynamics is positively regulated by pJNK and PI3K, while CAPP is a negative regulator of pAKT under only TNF α stimulation (Fig 3Ai). In the initial phase, pAKT was majorly controlled by pJNK (Fig 3Ai), thus the drop in the pJNK contribution is reflected on the decreasing levels in the initial phase (up to 4 h) of the dynamics of pAKT (Fig 2Bi). At later time-points, both pJNK and PI3K mediated effects dominate over other fluxes, and overcome the CAPP facilitated inhibition to initiate the late phase activation of the pAKT dynamics (Figs 3Ai and 2Bi). Bcl2 protein does not influence pAKT level, as its activity is repressed by NF κ B (Fig 3Ai). However, under NF κ B inhibitory conditions (TPL and TNF α + TPL), Bcl2 induces a rapid increase in the reaction flux of pAKT (Fig 3Bi and 3Ci) during the initial phase (up to 2 h). This results in a sharp increase in the initial dynamics of pAKT (Fig 2Biv and 2Bvii). A comparison of the contributions to pAKT for only TNF α stimulation (Fig 3Ai) and those with TPL stimulation (Fig 3Bi and 3Ci) suggests that pJNK contributions increased relatively as a result of NF κ B inhibition. However, PI3K contribution is completely lost, which can be attributed to the absence of NF κ B inhibition of PTEN (Fig 3Bi and 3Ci). This re-balancing of fluxes ensures a sustained maintenance of the pAKT dynamics at the later phase (Fig 2Biv and 2Bvii). In the case of only TPL, CAPP mediated inhibition of pAKT is insignificant (Fig 3Bi) as CAPP activation via Ceramide requires TNF α stimulation. Thus, pAKT levels in the case of TPL are higher compared to that of TNF α treatment. Since pAKT dynamics is primarily governed by TPL, the TNF α +TPL treatment as well shows higher pAKT levels as compared to only TNF α case.

The reaction flux investigation further indicates that C1P and MKK4/7 are the key controllers of pJNK dynamics, while XIAP/Gadd45B (XG) negatively influences it (Fig 3Aii, 3Bii and 3Cii). Our analysis reveals that initially the inhibitory effect of XG dominates over the contribution from any other nodes under only TNF α stimulation (Fig 3Aii), which creates a steep drop in the FC of pJNK (Fig 2Bii) in the early phase. In the later phase, the C1P and MKK4/7

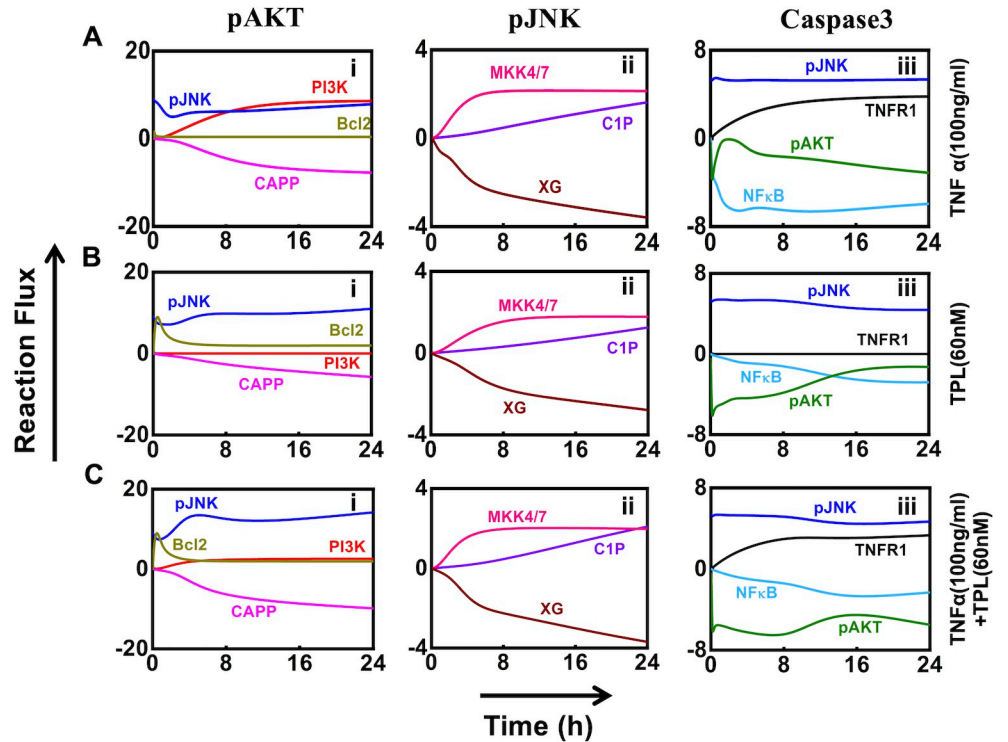


Fig 3. The evolution of majorly contributing fluxes towards pAKT, pJNK and Caspase3. Panels (A), (B), and (C), respectively show the evolution of fluxes for the three markers under the stimulation conditions TNF α , TPL, and TNF α + TPL. In each of the panels (i), (ii), and (iii), respectively show the evolution of fluxes contributing to dynamics of pAKT, pJNK and Caspase3 dynamics for the three different stimulation conditions. The individual reaction fluxes were estimated using the rate equation described in S4 Table. Evolution of all contributing fluxes has been presented in S10 Fig.

<https://doi.org/10.1371/journal.pcbi.1010626.g003>

primarily control the levels of pJNK (Fig 3Aii). However, in the presence of TPL, the inhibition by XG appears to be less effective (Fig 3Bii and 3Cii), which helps to stimulate the dynamics of pJNK at early time points (Fig 2Bv and 2Bviii).

Flux analysis further unfolds that NF κ B and pAKT are the major negative regulators of Caspase3 dynamics, while pJNK and TNFR1 are its positive modulators (Fig 3Aiii, 3Biii and 3Ciii). When stimulated with only TNF α (Fig 3Aiii), the balance between the predominant inhibition by NF κ B and mutual activation mediated by TNFR1 along with pJNK aid in maintaining sustained levels of Caspase3 (Fig 2Biii). Under TPL treatment, the initial dynamics of Caspase3 seems to be influenced both negatively by pAKT and positively by pJNK (Fig 3Biii) resulting in no activation of Caspase3 at the early phase (~8h) (Fig 2Bvi). As the later phase depicts a reduced pAKT inhibitory contribution towards Caspase3 flux (Fig 3Biii), there is an augmentation in the level of Caspase3 dynamics (Fig 2Bvi). Under the influence of TPL in the absence (Fig 3Biii) and presence (Fig 3Ciii) of TNF α , the contribution from NF κ B reduced significantly, while pAKT plays a predominant role in maintaining the dynamics of Caspase3 (Fig 2Bix). The inhibition mediated by pAKT was relatively less effective and thereby, controls the threshold extent of Caspase3 protein resulting in a sudden increase in its level (S10 Fig). Note that the positive contribution via pJNK helps in maintaining the sustained levels of Caspase3 under all three stimulation conditions (Fig 3Aiii, 3Biii and 3Ciii). However, for TNF α + TPL condition, the negative contribution of pAKT on Caspase3 dynamics starts increasing after 10h (Fig 3Ciii), leading to a gradual decrease in the Caspase3 levels (Fig 2Bix) during the later phase (16–24 h).

In summary, there is a signaling cross-talk between the pAKT and pJNK dynamics which in coordination with NF κ B regulates the Caspase3 dynamics. However, our flux analysis does not clearly identify how the signals originating from the TNFR1 and due to TPL pre-stimulation are channeled through various branches in order to orchestrate the pAKT and pJNK transients mediated synergistic signaling response to Caspase3.

Branch analysis reveals the synergistic dynamic cross-talk signaling regulating Caspase3 transients

We next perform a systematic branch analysis to distil out the extent of synergism exhibited in the dynamics of the signaling entities (pAKT and pJNK) based on the three stimulation conditions. First, we identify the branches originating from TNFR1 or NF κ B and ending in pAKT or pJNK (Tables 1 and S5). We analyze the relative capacity to process the signal flow through these branches for an i^{th} stimulation condition, where i stands for TNF α , TPL, or TNF α +TPL. The relative capacity (\mathbb{R}) of a branch, say, NF κ B \rightarrow pAKT (B_{na1} , Table 1), to process signal during i^{th} stimulation is given by

$$\mathbb{R}_{NF\kappa B \rightarrow pAKT} |_i = (J_{NF\kappa B \rightarrow pTEN} \times C_{pTEN})_i \times (J_{pTEN \rightarrow PI3K} \times C_{PI3K})_i \times (J_{PI3K \rightarrow pAKT} \times C_{pAKT})_i \quad (1)$$

where, $J_{l \rightarrow k}$ captures the absolute flux flowing along the interaction from l to k . C_k , the relative flux processing capacity of node k , is given by

$$C_k = \frac{\sum_{\forall n,m} J_{n \rightarrow m}}{\sum_{\forall p,n} J_{p \rightarrow n}} \quad (2)$$

where n , m and p is an index for the entities of the network (Fig 2B). We define extent of synergism (\mathbb{S}) facilitated by B_{na1} as

$$\mathbb{S}_{NF\kappa B \rightarrow pAKT} = \frac{\mathbb{R}_{NF\kappa B \rightarrow pAKT} |_{TNF\alpha + TPL}}{\mathbb{R}_{NF\kappa B \rightarrow pAKT} |_{TNF\alpha} + \mathbb{R}_{NF\kappa B \rightarrow pAKT} |_{TPL}} - 1. \quad (3)$$

Note that, for a given branch, $\mathbb{S} > 0$ and $\mathbb{S} < 0$, respectively indicate positive and negative synergism. We estimated the extent of synergism for all branches in Tables 1 and S5.

Table 1. Major branches originating from NF κ B or TNFR1 and ending in the signaling entities pAKT or pJNK. Comprehensive list of all branches are presented in S5 Table.

| ID | Branch |
|-----------|---|
| B_{na1} | NF κ B \rightarrow PTEN \rightarrow PI3K \rightarrow AKT |
| B_{na2} | NF κ B \rightarrow XG \rightarrow JNK \rightarrow AKT |
| B_{na3} | NF κ B \rightarrow PTEN \rightarrow PI3K \rightarrow ERK1/2 \rightarrow JNK \rightarrow AKT |
| B_{ta1} | TNFR1a \rightarrow PI3K \rightarrow AKT |
| B_{ta2} | TNFR1a \rightarrow RAF \rightarrow ERK1/2 \rightarrow JNK \rightarrow AKT |
| B_{ta3} | TNFR1a \rightarrow Ceramide \rightarrow C1P \rightarrow JNK \rightarrow AKT |
| B_{nj1} | NF κ B \rightarrow XG \rightarrow JNK |
| B_{nj2} | NF κ B \rightarrow Bcl-2 \rightarrow AKT \rightarrow MKK4/7 \rightarrow JNK |
| B_{nj3} | NF κ B \rightarrow PTEN \rightarrow PI3K \rightarrow Ceramide \rightarrow C1P \rightarrow JNK |
| B_{nj4} | NF κ B \rightarrow Bcl-2 \rightarrow AKT \rightarrow RAF \rightarrow ERK1/2 \rightarrow JNK |
| B_{ij1} | TNFR1a \rightarrow RAF \rightarrow ERK1/2 \rightarrow JNK |
| B_{ij2} | TNFR1a \rightarrow Ceramide \rightarrow C1P \rightarrow JNK |
| B_{ij3} | TNFR1a \rightarrow Ceramide \rightarrow CAPP \rightarrow AKT \rightarrow RAF \rightarrow ERK1/2 \rightarrow JNK |

<https://doi.org/10.1371/journal.pcbi.1010626.t001>

We present the dynamic variation of the extent of synergism facilitated by major branches (Table 1) in Fig 4. Branch B_{na1} originating from NF κ B offers positive synergism in the early phase and switches to negative synergism beyond 8 hours (Fig 4A, red). In particular, this positive synergism corresponds to the early rise of pAKT transient response for the TNF α +TPL case (Fig 2Bvii), which could be attributed to the effect of TPL via PI3K. On the other hand, the negative synergism in the later phase correlates with the drop in the pAKT response induced by TPL. While branch B_{na2} is responsible for maintaining the pAKT levels in the later phase, B_{na3} enables the early phase contributions of pJNK to pAKT transients (Fig 4A, blue and green). The undulations in the pAKT transients (Fig 2B) are due to the dynamic variation in the extent of positive synergism via branches B_{ta2} and B_{ta3} , both originating from TNFR1 (Fig 4B, gray and purple). These undulations are perhaps caused by the positive feedback loop involving RAF, ERK and JNK embedded in B_{ta2} (Table 1). The early phase switch in the synergism enabled by the branch B_{ta1} highlights the TNF α mediated signaling to pAKT via PI3K (Fig 4B, turquoise).

The steady marginal negative synergism via branch B_{nj1} is responsible for maintaining the JNK levels at later time points (Fig 4C, dark brown). On the other hand, the time-dependent undulated positive synergism observed in branches B_{nj2} and B_{nj3} (Fig 4C, light brown and dark blue) is manifested in the pJNK transients (Fig 2Bv and 2Bviii). The presence of RAF-ERK-JNK positive feedback in branch B_{nj4} (Table 1) could have resulted in the multiple rise and drop of synergism (Fig 4C, dark green). The nature of synergistic dynamics observed in B_{nj4} indicates a weak representation of this branch in the overall pJNK transient. This is due

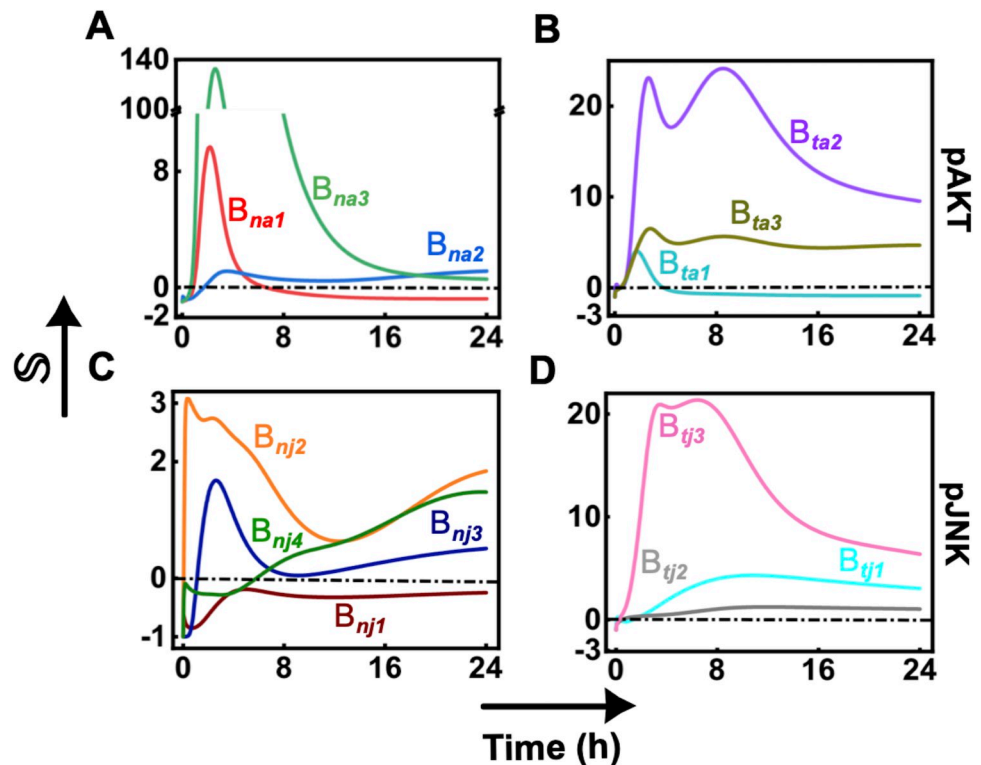


Fig 4. Dynamic evolution of the extent of synergism (S , defined in Eq 3) facilitated by major branches as depicted in Table 1. Synergism ($S > 0$ is positive and < 0 is negative) quantified from major branches originating from NF κ B to (A) pAKT and (B) pJNK, and that from TNFR1 to (B) pAKT and (D) pJNK. The evolution for other branches (S Table) are shown in S11 Fig.

<https://doi.org/10.1371/journal.pcbi.1010626.g004>

to the poor estimation of the kinetic parameters (such as K_{mae} , K_{eir} , and K_{air}) involved in the RAF-ERK-JNK feedback loop, which could explain the qualitative difference between the model fitting and experimental observations for pJNK under TNF α +TPL condition. Signal via branch B_{tj1} and B_{tj2} , both originating from TNFR1 maintain the initial basal pJNK transient levels in a synergistic manner (Fig 4D, turquoise and pink). Moreover, the signal flow via branch B_{tj3} contributes to keeping the transient pJNK levels high at the later phase (Fig 4D, dark blue). Contributions due to the remaining branches are elucidated in S5 Text and S11 Fig.

Overall the branch analysis elucidates how the transient pAKT and pJNK are governed by signal flow through different major branches in the TNF α signaling network (Fig 2A). This further confirms that a simple coarse-grained network in Fig 1A cannot capture the intricate dynamic signaling cross-talk and the synergism orchestrating the pAKT and pJNK dynamics. However, since branch analysis compares the relative signal flow due to multiple stimulation conditions, it cannot be employed to identify how the Caspase3 transient dynamics is precisely controlled by the pAKT and pJNK. In order to decipher this control, we next perform a time-dependent correlation analysis under the three stimulation conditions.

Dynamic correlation between pJNK and pAKT levels modulates overall Caspase3 transient response

The cooperative influence of pJNK and pAKT over Caspase3 transients need not necessarily be instantaneous and could be over an extended period of time. pAKT and pJNK accumulated over an extended period may coordinate in a time-dependent manner to control the overall Caspase3 levels along with the apoptotic response. We perform a systematic time-dependent correlation analysis of the accumulated levels of pAKT and pJNK to decipher the underlying regulation under different stimulation conditions. The accumulation of pAKT and pJNK are quantified by estimating the Area Under the Curve (AUC) of their transient responses (Methods) over different phases of the dynamics. In particular, we consider accumulation from the start (0 h) of the stimulation up to 8h, 12h and 24h for the correlation analysis. Note that the transients generated using the model for 5 best fit parameter sets were employed for this purpose.

The average relative contributions of accumulated pAKT (A_{pAKT}) and pJNK (A_{pJNK}) to overall Caspase3 levels are defined respectively by Eqs (7) and (8) in Methods. The relative contributions for the three stimulated conditions are presented in Fig 5A. When cells were stimulated with just TNF α , pJNK primarily contributes to the Caspase3 accumulated over various time durations (Fig 5Ai, shaded bars). Under TPL condition, pAKT dominates the Caspase3 accumulation for the first 8h (Fig 5Aii, unfilled bars). On the other hand, pJNK, which promotes Caspase3 activation, contributed negatively to Caspase3 accumulation (Fig 5Aii, shaded bars). Accumulation up to 12h shifted the pJNK contribution from negative to positive, while pAKT contribution decreased (Fig 5Aii). Subsequently, the influence of these two entities on overall Caspase3 level up to 24h becomes poised (Fig 5Aii). In the case of TNF α +TPL, the positive contribution from pJNK towards Caspase3 accumulation over 8, 12 and 24h increases along with a decrease in the impact of pAKT on it (Fig 5Aiii). This indicates that pJNK plays a significant role in regulating Caspase3 expression throughout the entire time course under all three stimulation conditions except during the initial phase for only TPL treatment.

Since Caspase3 along with other effector caspases such as Caspase7 are known to initiate apoptotic response [22], we determine how apoptosis is reflected in the overall Caspase3 accumulation (AUC_{casp3}) under these three stimulation conditions (Fig 5B). First, we analyze the

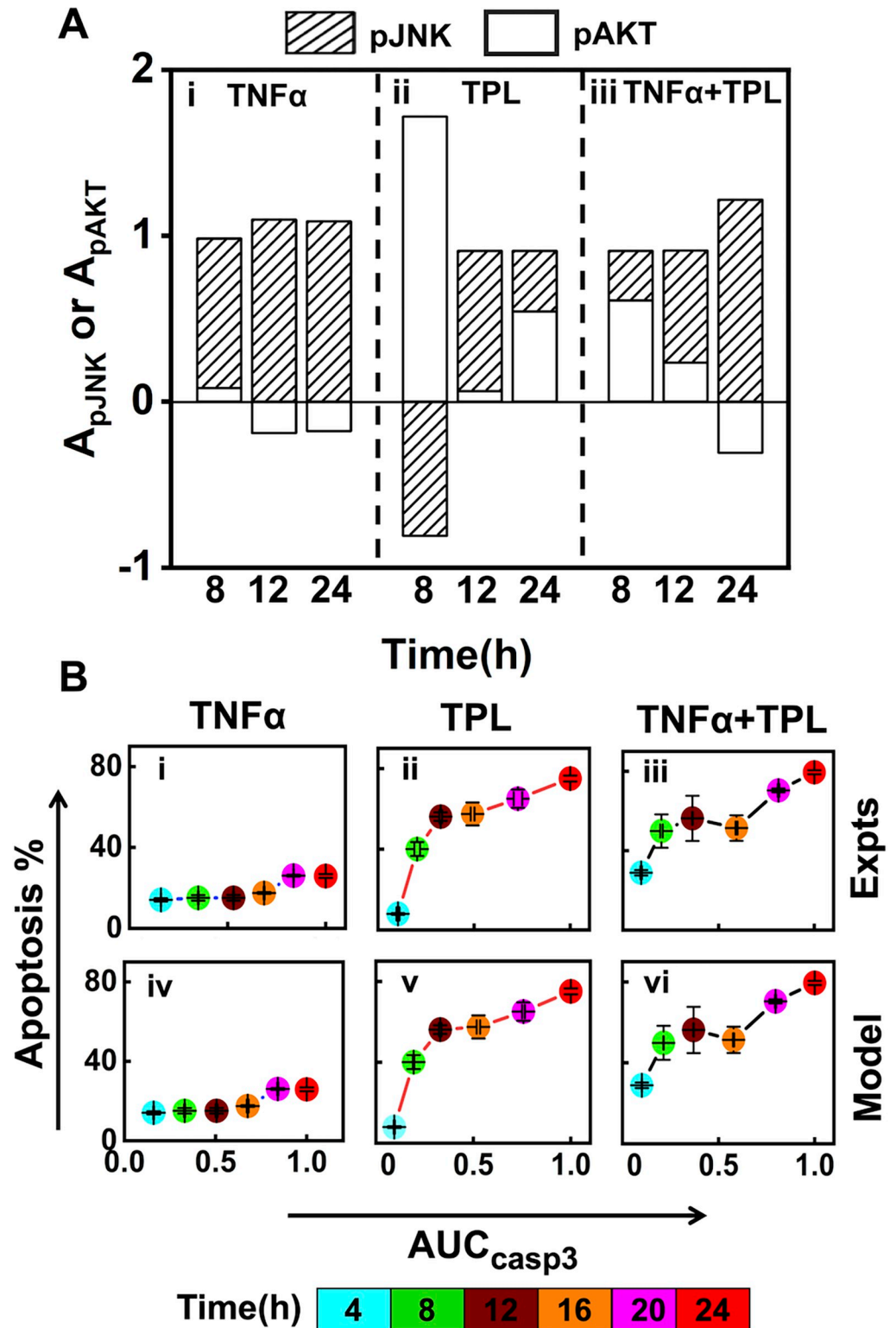


Fig 5. pJNK and pAKT transients synergistically control the overall Caspase3 levels and modulate the apoptotic response. (A) Relative contribution of model generated pJNK and pAKT transients corresponding to 5 best fit parameter sets (A_{pJNK} and A_{pAKT}) towards the corresponding overall Caspase3 accumulation for 8, 12 and 24 h durations for (i) TNF α , (ii) TPL, (iii) TNF α + TPL stimulation. (B) Depicts the correlation of experimentally measured accumulated Caspase3 levels (AUC_{casp3}) (n = 3) with corresponding apoptosis percentage for the stimulation conditions

(i) TNF α , (ii) TPL, (iii) TNF α + TPL. (iv-vi) represent correlation of model predicted accumulated Caspase3 levels (AUC_{casp3}) (n = 5) with the experimentally measured apoptosis percentage (n = 3) for the three stimulation conditions. The time points are appropriately color-coded in (B).

<https://doi.org/10.1371/journal.pcbi.1010626.g005>

experimentally measured apoptosis levels (Fig 1A) with the corresponding accumulated Caspase3 (Fig 1Ciii). For TNF α stimulation condition, the apoptosis percentage did not rise concomitantly with the increasing AUC_{casp3} (Fig 5Bi). This could probably be due to the activation of the survival pathway (NF κ B), which interferes with the apoptosis process (Fig 2A). When the NF κ B mediated survival signals are interrupted using TPL, there was an enhancement of Caspase3 accumulation over a 24h time period with an increase in the apoptosis level (Fig 5Bii). Moreover, the proportion of cells undergoing apoptosis increased monotonically with Caspase3 accumulation until 12 hours, following which no substantial rise in apoptosis (50% to 80%) occurred with an increase in AUC_{casp3} (Fig 5Bii). Similar behavior was observed for the TNF α + TPL case as well (Fig 5Biii). A comparison of the early phase apoptosis response for the TPL (Fig 5Bii) and TNF α + TPL (Fig 5Biii) cases shows marginally higher percentage apoptotic response as that in the former. This suggests that Caspase3 accumulation up to a particular threshold at the early time point (4–12h) is a pre-requisite to commit cells for apoptosis, which is only moderately affected by the Caspase3 surge at later time points (24h) for U937 cells. Next, we show the experimentally observed apoptosis levels with the model-predicted overall Caspase3 accumulation (Fig 5Biv–5Bvi). A comparison of Fig 5Bi–5Biii and 5Biv–5Bvi demonstrates that the model simulated AUC_{casp3} predicts the apoptosis levels as good as that by those from experimental measurements. This suggests that even though the accumulation information was *not* considered in the model training process (Fig 2B), the transients generated using the estimated model parameters adequately captures the apoptosis response via AUC_{casp3} . In summary, both pJNK and pAKT, and their coordinated cross-talk with the NF κ B regulation finetunes the apoptotic response by modulating the overall Caspase3 levels.

Inhibiting pAKT and pJNK signaling alters Caspase3 transient response

Dynamic correlation analysis (previous section) suggests that fine-tuning the apoptotic response could be achieved by altering the overall Caspase3 dynamics by perturbing the pAKT and pJNK transients. We introduce these perturbations by exposing U937 cells to either Wortmannin (Wort) or SP600125 (SP6). Wort inhibits PI3K mediated pAKT activation (Fig 6A) [61,62], pJNK activation through MKK4/7 [63–65] and XG activation through NF κ B [66]. On the other hand, SP6 affects both pJNK and pAKT activation via different pathways (Fig 6B) [67]. SP6 further activates Caspase3 [68] by down regulating Bcl2 activation leading to reduction in pAKT levels and inhibits MKK4/7 through the AP-1 and Fas driven pathway [67,69–73]. We incorporate these perturbations using phenomenological terms in the model, which will henceforth be referred to as *inhibitory model*. (Details of inhibitory model are described in S6 Text.)

We first consider the case of Wort inhibition in our model simulations, which demonstrate that after a transient initial peak, pAKT levels decrease with time under all three stimulation conditions (Fig 6Ci). This could be due to pJNK playing a significant role in activating pAKT (Fig 2A). On the contrary, for all three stimulation conditions, after an initial dip, pJNK dynamics showed a steady increasing trend with an undulation (Fig 6Cii). This could be due to the RAF-ERK-JNK feedback loop identified using the branch analysis (Fig 4C and 4D and Table 1). For the case of only TNF α , in the presence of Wort, model predicts a marginal increase in Caspase3 level (Fig 6Ciii, blue cloud). However, when stimulated only with TPL or TNF α +TPL, simulations showed a gradual time-dependent increase in the Caspase3 levels

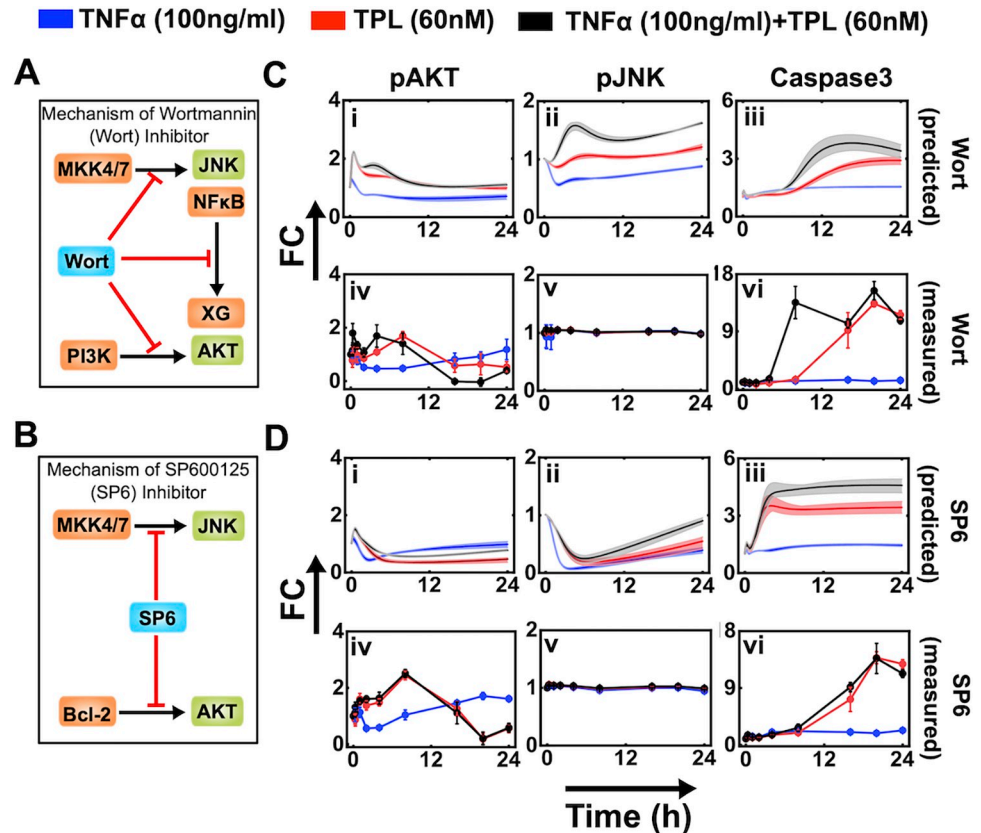


Fig 6. Model prediction and experimental validation of the marker proteins under the treatment of Wortmannin (Wort) and SP600125 (SP6) inhibitor. (A) and (B), respectively schematically represents the inhibitory action of Wort and SP6. (C) Effect of Wort inhibition on (i) pAKT, (ii) pJNK, and (iii) Caspase3 as predicted by model simulations. The corresponding experimental validations are in (iv), (v), and (vi), respectively. (D) Effect of SP6 inhibition on (i) pAKT, (ii) pJNK, and (iii) Caspase3 as predicted by model simulations. The corresponding experimental validations are in (iv), (v), and (vi), respectively. The rate constant values used for the inhibitory interactions are given in the caption of S12 and S13 Figs.

<https://doi.org/10.1371/journal.pcbi.1010626.g006>

from the initial phase (Fig 6Ciii, red and black clouds). The flux analysis (S12 Fig) demonstrates that the effect of Wort reduces the inhibitory contributions of pAKT and NFkB fluxes over Caspase3 dynamics. For all three stimulation conditions, the levels reached in the initial phase subsequently settles into the corresponding steady level by 24 hours (Fig 6Ciii). To validate these model predictions, we measured the transient levels of pAKT, pJNK and Caspase3 in Wort treated U937 cells under all three stimulation conditions (Fig 6Civ–6Cvi). (A comparison of the model predictions and the corresponding measurements with those obtained for the case of no Wort inhibition is presented in S6 Text.) The experimentally measured pAKT and Caspase3 dynamics corroborated qualitatively with the theoretical model predictions (Fig 6Ci, 6Ciii, 6Civ and 6Cvi). However, the sustained very low fold-change detected experimentally for pJNK could not be predicted by the model simulations (Fig 6Cii and 6Cv), which we attribute to poor estimation of certain kinetic parameters related to a major branch involving RAF-ERK-JNK feedback loop.

We next investigate the effect of SP6 inhibition. The model predicted trend for pAKT, pJNK and Caspase3 were by and large similar to those obtained for the case of Wort inhibition for respective stimulation conditions (Fig 6Di–6Diii). (Inhibitory model predictions along with the experimental measurements under three different stimulation conditions are

contrasted with those obtained for the case sans SP6 inhibition in [S12 Fig](#)) The experimentally measured dynamics of these proteins in SP6 treated U937 cells qualitatively substantiate the model predictions for all three stimulation conditions ([Fig 6Div–6Dvi](#)). Specifically, for the TPL and TNF α +TPL stimulation conditions, the rise in the Caspase3 levels were delayed as compared to model simulations ([Fig 6Diii and 6Dvi](#)).

Flux analysis of the inhibitory model simulations ([S6 Text](#)) revealed that in the presence of Wort, weak inhibition of JNK activation by MKK4/7 was required to capture the qualitative experimental trend of Caspase3 and pAKT transients. Activation of JNK is primarily caused by MKK4/7 and C1P under normal conditions ([Fig 3Aii, 3Bii and 3Cii](#)). Under Wort inhibitory conditions, the fluxes to JNK from these interactions almost remained unaltered ([S12 Fig, ii, v, viii](#)) leading to poor model prediction of pJNK dynamics. Experiments show that transient Caspase3 rise correlates with drop in the pAKT transient under TPL and TNF α +TPL conditions. However, for these two conditions, in the model predictions, the pAKT transients are maintained at a higher steady-level, which is above that for the case of only TNF α treatment. This is the reason why the model underestimates the relative rise in the Caspase3 transients for TPL and TNF α +TPL treatment under Wort inhibitory conditions. Flux due to pJNK maintains a higher pAKT level at later time points ([S12 Fig, i, iv, vii](#)). On the other hand, in the case of SP6 mediated inhibition, the flux analysis reveals that MKK4/7 mediated pJNK activation is completely shut down causing the early phase dip in pJNK and thereby in pAKT transients as well ([S13 Fig, ii, v, viii](#)). As a consequence, the model predicts the rise in the Caspase3 dynamics occurring much earlier than that observed in experiments ([Fig 6Diii](#)). Moreover, for TPL and TNF α +TPL cases, except TNFR1 mediated Caspase3 activation, all other fluxes contribute to Caspase3 transients in a similar manner ([Fig 6Diii](#)). This substantiates the experimentally observed fact ([Fig 6Div](#)) that the Caspase3 transients are similar for TPL and TNF α +TPL treatments.

Overall, our model could qualitatively predict the modulation in Caspase3 dynamic response under all the three experimental conditions (TNF α , TPL and TNF α +TPL) in the presence of either Wort or SP6 inhibitor as substantiated by the experimental data. Thus, model is able to predict the cell-fate decision in U937 cells for which the AUC_{casp3} can act as a suitable intracellular signature. This leads to the hypothesis that fine-tuning apoptosis can be achieved by controlling AUC_{casp3} .

Model adequately predicts apoptotic response in U937 cells under all stimulation conditions

In order to test the above hypothesis, we contrast the model predicted apoptotic response with those observed experimentally when U937 cells are treated with Wort or SP6 inhibitors under all three stimulation conditions (TNF α , TPL, TNF α +TPL). For predicting apoptosis level using the model simulated AUC_{casp3} at a certain time, we assume the correlation between AUC_{casp3} and apoptosis in [Fig 5Biv–5Bvi](#) as a calibration for the three stimulation conditions. (Note that the inhibitory action via Wort or SP6 are on signaling entities upstream of Caspase3. Therefore, the relationship obtained between the AUC_{casp3} and apoptosis under non-inhibitory conditions ([Fig 5Biv–5Bvi](#)) would continue to hold under inhibitory conditions as well.) In order to find the apoptotic response for the entire range of AUC_{casp3} in [Fig 5Biv–5Bvi](#), we quantify the correlation between model generated AUC_{casp3} vs experimentally observed apoptosis using a polynomial curve fit. (Details of the fit and identifiability of the associated parameters are provided in [S7 Text](#) and [S6 Table](#).) Note that the curve fitting was performed using the $\langle AUC_{casp3} \rangle$, which is an average over that estimated using five best-fit model simulated trajectories. Next, using the Wort or SP6 inhibitory model simulations, for a certain time

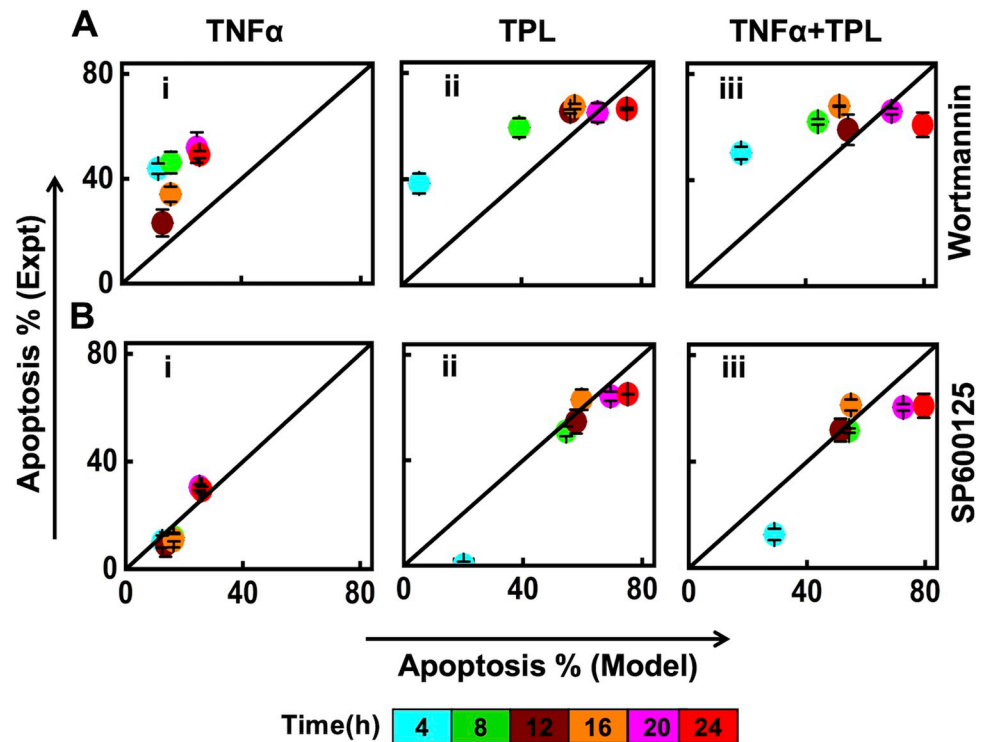


Fig 7. Comparison of experimental and model predicted apoptosis percentage under (A) Wort and (B) SP6 inhibitory conditions. (i), (ii), and (iii), respectively correspond to the predictions for TNF α , TPL, and TNF α + TPL stimulation conditions. While 5 best fit parameters were considered for model predictions, those of experiments are based on triplicates. The time points are appropriately color-coded in (B).

<https://doi.org/10.1371/journal.pcbi.1010626.g007>

duration under a specific stimulation condition, we estimated the $\langle AUC_{casp3} \rangle$, which was incorporated in the polynomial fit to arrive at the model predicted apoptosis percentage (Fig 7). The corresponding apoptosis percentage in U937 cells was measured experimentally (Methods).

For the Wort inhibition case under only TNF α stimulation condition, the model under-predicted the experimentally observed apoptosis percentage (Fig 7Ai). This is due to poor prediction of the pJNK level by the Wort inhibitory model (Fig 6Aii, blue). This deviation is reflected in the lower levels of Caspase3 transient (Fig 6Aiii, blue) causing decreased $\langle AUC_{casp3} \rangle$. For the TPL and TNF α + TPL cases (Fig 7Aii–7Aiii), the Wort inhibitory model predicts the experimental apoptosis percentage at all time durations other than 4h. Note that after 16h the experimental apoptosis levels become insensitive to the marginal increment in $\langle AUC_{casp3} \rangle$ under both these conditions (Fig 7Aiii).

The SP6 inhibitory model predicted apoptosis levels match the experimental apoptotic measurements in U937 cells for all the time points during only TNF α stimulation (Fig 7Bi). For the case of TPL and TNF α + TPL stimulations, for intermediate time points (8, 12, 16h), the experimental observations corroborate model predictions (Fig 7Bii and 7Biii). However, for these two conditions, the model over-predicts the apoptosis levels at earlier and later duration. The over-prediction at the early time point (4 h) could be due to model predicting significantly higher levels of initial Caspase3 transients as compared to the experimental observations (Fig 6Biii and 6Biv). Experimentally observed apoptosis response being insensitive to accumulated Caspase3 levels (Fig 7Bii and 7Biii) could explain the overprediction by the model at later time points (Fig 6Diii). Juxtaposition of model predicted $\langle AUC_{casp3} \rangle$ and

apoptosis leading to a correlation can help contrasting the experimentally observed and model simulation predicted apoptotic cell-fate response. Such a comparison can be achieved by inhibiting other entities in the network as well.

Discussion and conclusion

Dynamic crosstalk among intracellular signaling entities plays a crucial role in regulating the cell-fate as a response to the pleiotropic cytokine TNF α stimulation. In this study, we present an experimental data-constrained mathematical model consisting of 17 entities and 25 interactions that can predict the apoptotic response under different physiological conditions related to TNF α signaling network. The experimental data represents the dynamical response due to activation of signaling pathways downstream of TNFR1 stimulated by the soluble 17.3 kDa TNF α . (Note that signaling due to TNFR2, activated only by 26 kDa transmembrane TNF α , and its downstream signaling are ignored.) Using systems biology-based approaches, we unravel the synergistic interdependence of pAKT and pJNK transient response and their dynamic cross-talk modulating apoptosis via Caspase3 dynamics in U937 cells in a semi-quantitative manner.

While TNF α signaling maintains a delicate balance between the survival and apoptotic responses [10], tilting the balance towards apoptosis by inhibiting signaling downstream NF κ B has been demonstrated [74]. There are several interconnected signaling branches that could influence this cell-death decision [75]. Our experimental findings unfold that arresting survival signaling via NF κ B pathway using Triptolide (TPL) aided in quantifying the transient influence of pJNK and pAKT activity on the apoptotic response in U937 cells (Figs 1 and 5A). The delayed Caspase3 response observed in our experiments and predicted by the model is in line with those reported in other cell lines [76]. By monitoring NF κ B and Caspase signaling for just 1–2 hours, Lee *et al.* revealed that a 1-min TNF α pulse can be more efficient at killing cells than a 1-hour pulse [46]. Timescale of apoptotic response and the upstream signaling influencing the same is cell-type specific. Our model analysis revealed that the nature of influence of the transients of the signaling entities on cell-death is time-dependent.

For U937 cells, we identified that the influence in the early phase (< 8 hours) is distinct to that in the late phase (8 to 24 hours) (Fig 8). This was deciphered by tracking the nature of synergism in signal flow via different branches using the branch analysis (Fig 4). For example, the signal transduction requires NF κ B \rightarrow pAKT branch to dynamically switch from a positive to negative synergism across the two phases (Fig 8). The low Caspase3 levels at the early phase and the subsequent rise in the late phase (Fig 2) can be attributed to the early phase negative synergism in the NF κ B \rightarrow pJNK branch being absent in the late phase (Fig 8). Moreover, the positive synergism elicited by the branches originating from TNFR1 involving the RAF-ERK1/2-JNK positive feedback loop influences the dynamics of pAKT in both early and late phases (Fig 8). Combined effect of the dynamically varying synergism in these branches governs the Caspase3 transients via pAKT and pJNK, and therefore the phenotypic apoptotic response (Fig 5B).

Traditional approach of discrete-level modeling identified that pJNK and pAKT can influence the TNF α mediated apoptotic response but does not lead to precise extent of dynamic cross-talk [43,44]. The reaction flux analysis along with the branch analysis revealed the causal mechanism regulating apoptotic response involving the dynamic cross-talks among the key intracellular entities pJNK and pAKT (Figs 3 and 4). We identified that pJNK transient response and PI3K play crucial roles in controlling pAKT dynamics. While PI3K primarily influences the late-phase activation of pAKT, pJNK affects it over the entire 24 h duration (Fig 3). Such a different early and late-phase responses of the marker proteins have also been observed during p53 signaling induced by DNA damage response [77–80].

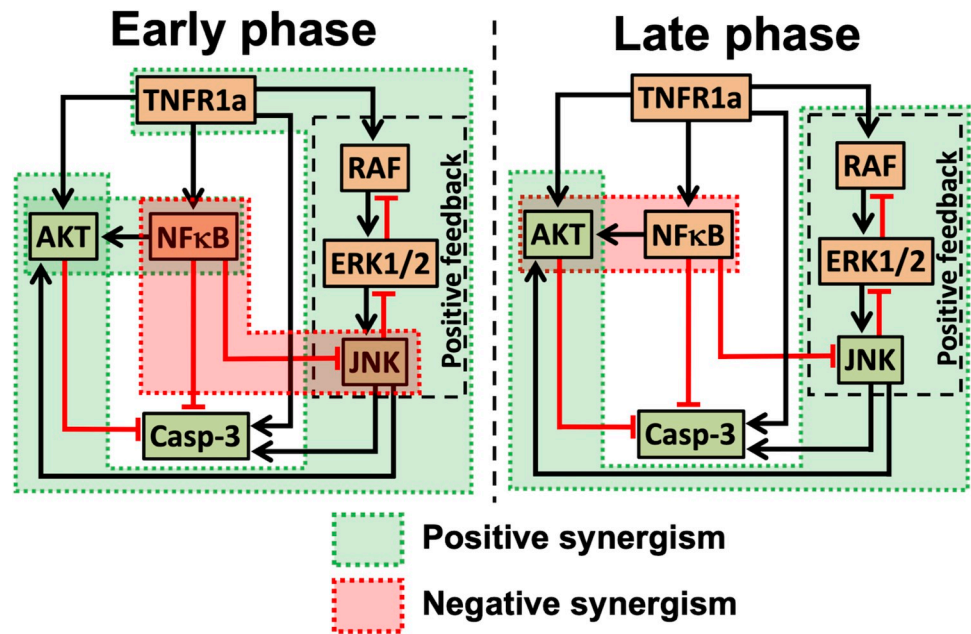


Fig 8. Comparison of time-dependent synergism during the early and late phase signaling cross-talk regulating Caspase3 activation.

<https://doi.org/10.1371/journal.pcbi.1010626.g008>

Since cell-death is a long-term phenotypic response, identifying the quantitative relationship between the intracellular marker levels and the apoptosis can offer strategies for its modulation. Contrary to that observed experimentally, TNF α network model developed by Koh and Lee predicted that Caspase3 activation predominates at short timescales post-stimulation [81]. This could be attributed to not considering pJNK, which is a crucial Caspase3 regulator, as shown by our predictions (Fig 5A). While arresting the pro-survival pathways is expected to alter the cell-death decisions [82,83], our study demonstrates that a semi-quantitative correlation establishes the connection between the Caspase3 dynamics and the apoptotic response (Fig 5B). The premise of this correlation is to relate the Caspase3 levels over a range of time duration represented by accumulated levels to the phenotypic response. Therefore, the correlation can serve as a guide for modulating the TNF α mediated cell-death behavior.

Correlation between the model simulated accumulated Caspase3 levels and experimentally detected apoptosis response enabled prediction of apoptotic phenotype in the presence of Wortmannin and SP600125 inhibitors (Fig 6). Even though the phenotypic predictions are valid only in the range of the accumulated Caspase3 levels, the systematic semi-quantitative approach employed can be easily extended to other perturbative conditions. While this approach can help gain insights into various therapeutic responses, there is a scope for further refining the model for improving its predictive abilities. For example, the model did not adequately predict the pJNK transient behavior (Fig 2). This can perhaps be reconciled by introducing additional pJNK regulating nodes or interactions. Cell-to-cell variability is inherently present even in our experimental measurements (S1 Text). However, our model, due to its deterministic nature, is not appropriate to mimic such variabilities. Recent studies have indeed shown that superimposing stochasticity on a deterministic model could allow accounting for cell-to-cell variability [45,84]. Thus, the model proposed here can be extended to capture the ensemble-level behavior. Overall, we demonstrate that predicting the synergistic cross-talk signaling guided qualitative apoptotic phenotypic response is possible even without capturing the detailed pathway of apoptosis in an explicit manner.

Materials and methods

M1. Cell culture and reagents

U937 cells were procured from the Cell Repository at National Centre for Cell Science (NCCS), Pune, India. It was cultured in RPMI-1640, supplemented with 10% fetal bovine serum (FBS), 2 mmol/l L-glutamine, and 1% antibiotic-antimycotic solution, all procured from HiMedia (Mumbai, India) with a cell-seeding density of 5×10^5 cells/ml. Cells were then collected, pelleted by centrifugation at 1,000 rpm for 5 min at room temperature (RT) and maintained at 37°C in a humidified 5% CO₂ incubator. 17.3kDa TNF α (Peprotech) was reconstituted in double-distilled water to a concentration of 100 μ g/ml. Triptolide (TPL) (Sigma) was dissolved in DMSO to a concentration of 1 mg/ml, the stock was stored at -20°C until use. Antibodies against different proteins ((phospho-pAKT(pS473)- Alexa 488-tagged antibody, phospho-pJNK(pT183/pY185)- PE tagged, and anti-active Caspase3- V450 tagged antibody)) were procured from BD Biosciences.

M2. Apoptosis detection using Annexin V/PI staining

U937 cells were plated in 24-well plates. For a certain experimental condition, cells in different wells were treated with the corresponding stimulation for 4, 8, 12, 16, 20 or 24 h. For those conditions involving TPL, cells were pre-treated with it for 1 h prior to TNF α addition. After the completion of the stimulation time, cells were harvested, washed once with PBS, resuspended in 1X Annexin binding buffer and stained with FITC-labeled Annexin V and PI (BD Pharmingen, San Diego, CA, US). Cells were then analyzed on BD FACS Aria (BD Biosciences, San Jose, CA, US) within 30 min of dye addition. For every experimental condition and time point, three replicates were used.

M3. Intracellular staining with Flowcytometry using Fluorescent Cell Barcoding (FCB)

U937 cells were seeded in 12 well plates for measuring signaling levels at 12 timepoints over a span of 24 h. For both TPL and TNF α + TPL stimulation conditions, cells were pre-treated with TPL for 1hr. After the stimulation, cells were fixed with 4% PFA for 10 min at RT, washed once with PBS and then transferred to a 96-well plate for further processing. Cells were then permeabilized with 500 μ l of 80% chilled methanol on ice for 1 h, and washed in PBS to remove leftover methanol. Now 50 μ l of 4 different concentrations (10 μ g/ml, 2 μ g/ml, 0.4 μ g/ml and 0.08 μ g/ml) of barcoding dye (Alexa-647) was added to the samples (450 μ l in PBS) making up the total volume to 500 μ l and kept on ice for 40min. After the incubation, cells were washed with 0.5%BSA in PBS to remove unbound dye. Finally, a combo tube was prepared that consisted of 4 different concentrations of the dye and washed thrice with 0.5%BSA in PBS to remove excess unbound dye. Cells resuspended in 0.5% BSA in PBS, were stained with antibodies against pAKT, pJNK and Caspase3 with dark incubation at RT for 30min. After removing the unbound antibody, cells resuspended in 300 μ l of 0.5% BSA were analyzed for detecting fluorescence in various channels on a BD FACS Aria flow cytometer. A schematic of this entire high-throughput protocol is in [Fig 9](#).

M4. Data quantification

The obtained file was then deconvoluted using FlowJo (version 10). Each fluorochrome used corresponds to a particular protein. Mean Fluorescence Intensity (MFI) of the distribution was used to calculate the relative fold change of the protein level upon stimulation. Relative

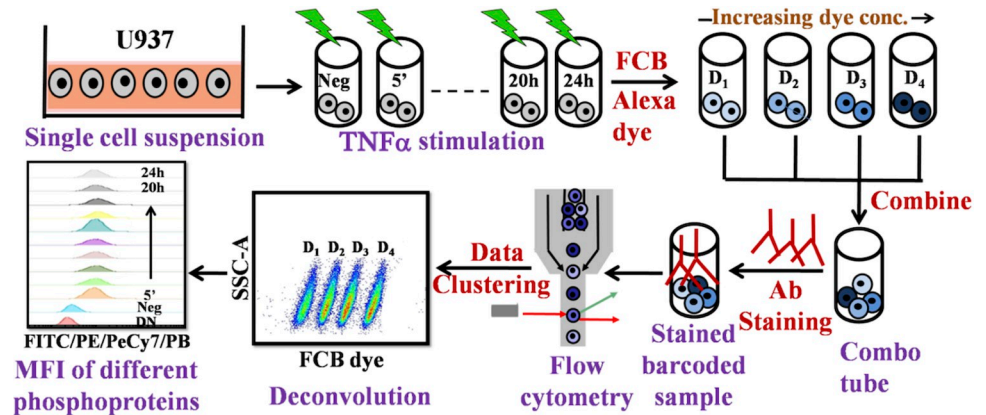


Fig 9. Schematic of high throughput signaling experimentation. Cells are harvested and incubated with inhibitor or stimulus for the desired time. After incubation, cells are fixed using paraformaldehyde and subsequently permeabilized with methanol. Four samples, each containing sufficient number of cells, are then incubated with amine-reactive fluorescent barcoding (FCB) [55,56] dye with different concentrations. These four samples are combined in a combo tube. After covalent binding, cells in the combo tube are washed several times to remove unbound dye, following which they are exposed to monoclonal antibody against the intracellular proteins. Fluorescence emitted by cells in the combo tube is then acquired on a flow cytometer. After acquisition, the samples are analyzed by gating and identifying individual samples displaying discrete fluorescent intensities (D1, D2, . . . D4) in the FCB channel. Mean fluorescent intensities of the fluorescence distribution corresponding to individual proteins are captured in different channels based on the fluorochrome antibody for further analysis.

<https://doi.org/10.1371/journal.pcbi.1010626.g009>

fold change (FC) at a certain time point is given by

$$FC = \frac{MFI_t - MFI_{DN}}{MFI_{Neg} - MFI_{DN}} \tag{4}$$

where, MFI_t , MFI_{Neg} , MFI_{DN} , respectively represent MFI at a certain time t , negative control (no stimulation (0 h)), and double negative (only cells).

M5. Signaling pathway perturbation with inhibitors

For each of the stimulation conditions, cells were treated with inhibitor Wortmannin (1 μ M) or SP600125 (10 μ M) for 1 h prior to stimulation. After treatment, cells were stained as per the method specified earlier. Further the fluorescence emitted by the stained samples were acquired using BD FACS Aria following which FC at the measured time points were estimated using Eq (4).

M6. Model kinetic parameter estimation

The model kinetic parameter estimation was performed using the PottersWheel software (version 4.1.1) [85] by employing “Trustregion” method with underlying ODEs integrated using CVODE method. The model system has been optimized ~2000 times by taking the same initial starting values of the parameters (parameters are globally fitted by considering a logarithmic parameter space) to fit the experimental data adequately. We considered χ^2 value for a certain parameter set P as the fitting criteria, where χ^2 is defined as

$$\chi^2(P) = \sum_{i=1}^N \left(\frac{y_{pAKT,i}^e - y_{pAKT}(t_i; P)}{\sigma^2} \right)^2 + \sum_{i=1}^N \left(\frac{y_{pJNK,i}^e - y_{pJNK}(t_i; P)}{\sigma^2} \right)^2 + \sum_{i=1}^N \left(\frac{y_{Casp3,i}^e - y_{Casp3}(t_i; P)}{\sigma^2} \right)^2 \tag{5}$$

where, $y_{pAKT,i}^e$, $y_{pJNK,i}^e$ and $y_{Casp3,i}^e$ represent the mean of the triplicate experimental FC data for the pAKT, pJNK, Caspase3, respectively at the i^{th} time point. $y_{pAKT}(t_i; P)$, $y_{pJNK}(t_i; P)$, and $y_{Casp3}(t_i; P)$ are the levels of the respective proteins at the i^{th} time point obtained from model simulations for a chosen parameter set P . σ is the standard deviation of the experimental data set. The detailed description of the model development is in [S2 Text](#).

M7. Reaction Flux analysis

For a certain node such as pAKT, the rate law corresponding to every incoming and outgoing interactions were evaluated at every time point. For a certain interaction, a locus of these over 24 h is its reaction flux trajectory. We repeated this procedure to find the reaction flux trajectories for the interactions in which pAKT, pJNK and Caspase3 are involved. Details of these are in [S4 Text](#).

M8. Branch identification

TNF α signaling network ([Fig 2A](#)) was converted into an unsigned, interaction digraph. Adjacency matrix for the digraph was generated. Subroutine 'allpaths.m' in Matlab was used to identify all paths (or branches) between a pair of entities. Subsequently, for every branch, interactions in it were assigned their respective sign (Tables [1](#) and [S5](#) as specified in the original network).

M9. Correlation analysis and Linear regression

For a certain stimulation condition, area under the curve (*AUC*) was calculated for pAKT, pJNK and Caspase3 transients up to 8, 12, and 24 h time durations. For model-based *AUC*, transients generated using 5 best parameter sets were employed. Linear regression (in R [[86](#)]) was carried out using the *AUC* from all 5 transients to find the constants a and b in overall pJNK and pAKT contributions in accumulated Caspase3 captured in

$$AUC_{casp3} = a \times AUC_{pJNK} + b \times AUC_{pAKT} \quad (6)$$

Relative contributions were estimated by normalizing all terms in Eq (3) with $\langle AUC_{casp3} \rangle$, the average of AUC_{casp3} across replicates. Thus, the average relative contributions of pAKT (A_{pAKT}) and pJNK (A_{pJNK}), respectively are defined as

$$A_{pAKT} = \left\langle \frac{b \times AUC_{pAKT}}{\langle AUC_{casp3} \rangle} \right\rangle \quad (7)$$

and

$$A_{pJNK} = \left\langle \frac{a \times AUC_{pJNK}}{\langle AUC_{casp3} \rangle} \right\rangle \quad (8)$$

where, $\langle . \rangle$ represents average across replicates. Note that $A_{pJNK} + A_{pAKT} = 1$.

Supporting information

S1 Text. Apoptosis and intracellular marker protein level detection.

(PDF)

S2 Text. Detailed model of the TNF α signaling network capturing the cross-talk between different entities.

(PDF)

S3 Text. Prediction and sensitivity analysis of transient dynamics of different entities from the proposed model.

(PDF)

S4 Text. Reaction flux analysis of the three marker proteins.

(PDF)

S5 Text. Branch analysis quantifying the synergistic dynamic cross-talk signaling.

(PDF)

S6 Text. Model analysis under inhibitory conditions—Wortmannin (Wort) and SP600125 (SP6).

(PDF)

S7 Text. Semi-quantitative relationship between $\langle AUC_{casp3} \rangle$ and Apoptosis levels.

(PDF)

S1 Fig. Effect of TPL on cell survival. (A) Dose-response of TPL on cell-survival. (B) Effect of TPL pre-treatment duration on apoptosis. Note that negative Apoptosis % in (B) for a few cases are due to negative control (only cells) being more than that when treated.

(TIFF)

S2 Fig. Detailed TNF α signaling network. Activation and inhibitory actions are represented by solid (black) and dashed (red) lines, respectively. Green and orange boxes, respectively represent the inactive and active forms of an entity. The model contains 34 species and 81 parameters including 3 scaling constants.

(TIFF)

S3 Fig. Generalized methodology to identify best suitable model based on goodness of fit.

The proposed models were mapped with experimental data and robust model was selected by performing parameter optimization and associated identifiability analysis.

(TIFF)

S4 Fig. Boxplot showing deviation of the estimated kinetic parameters around its median.

(TIFF)

S5 Fig. Model trajectories for best fitted parameter set with experimental measurements.

The best-fitted trajectories (red) of ~2000 fits with the experimental FC (circles with appropriate error bars) for pAKT, pJNK and Caspase3 under the three stimulation conditions. The errors are estimated by using a standard error model.

(TIFF)

S6 Fig. Model predicted time course simulation of fold activation (FC) of transient varying different concentrations of TNF α . Simulated trajectory of FC by varying TNF α in (A) the absence of TPL, (B) presence of low dose TPL (10nM) and (C) presence of high dose TPL (60nM).

(TIFF)

S7 Fig. NF κ B dynamics under different stimulation conditions. Trajectories of NF κ B protein obtained by simulating the model with best-fit parameter set ([S4 Table](#)).

(TIFF)

S8 Fig. Comparison of model predicted transients with experimental measurements for TPL-10nM in the presence of TNF α (100ng/ml). The green lines represent the simulated

trajectories and the black dots with corresponding error bars ($n = 3$) indicate the experimental measurements.

(TIFF)

S9 Fig. Relative influence of the cross-talk related parameters on the predicted dynamics for the case of TPL-10nM in the presence of TNF α (100ng/ml). Φ_k and Φ_{WT} , respectively captures the area under the transient for the case of deviation in a certain cross-talk parameter and that for the case of the best fit parameter. Note that a deviation of 20% (as specified in the third column of Table I in [S3 Text](#)) from the best fit values in Table I in [S3 Text](#) was considered for this analysis.

(TIFF)

S10 Fig. Temporal evolution of fluxes contributing to the dynamics of pAKT, pJNK and Caspase3 under the three stimulation conditions. Rows correspond to different stimulation conditions. Expression for these fluxes (A_i , J_i and C_i , for all i) are provided in [S4 Table](#).

(TIFF)

S11 Fig. Time-dependent synergism due to all branches from (A) NF κ B to pAKT, (B) TNFR1 to pAKT, (C) NF κ B to pJNK, and (D) TNFR1 to pJNK as listed in [S5 Table](#).

(TIFF)

S12 Fig. Evolution of fluxes from important entities controlling the dynamics of pAKT, pJNK and Caspase3 under different experimental conditions in the presence and absence of Wort inhibitor. Flux analysis of different nodes on controlling of pAKT, pJNK and Caspase3 under different experimental conditions in the presence of Wort inhibitor. The dotted line represents when simulation has been done at 0 nM (no inhibitor) of Wort and the solid line depicts the trajectories for 1000 nM of Wort. The contribution from each specific node in the time profile of marker protein has been dissected separately by considering various terms in the corresponding model equation in [S4 Table](#). Wherever necessary, the inhibitory action related modifications to the relevant rate terms were considered. Inhibitory parameters used are $K_{iak} = 0.001 \text{ nM}^{-1}$, $K_{kim} = 0.02 \text{ nM}^{-1}$, and $K_{kxg} = 0.00005 \text{ nM}^{-1}$.

(TIFF)

S13 Fig. Evolution of fluxes from important entities controlling the dynamics of pAKT, pJNK and Caspase3 under different experimental conditions in the presence and absence of SP6 inhibitor. Flux analysis of different nodes on controlling of pAKT, pJNK and Caspase3 under different experimental conditions in the presence of SP6 inhibitor. The dotted line represents when simulation has been done at 0 nM (no inhibitor) SP6 and the solid line depicts the trajectories for 10000 nM of SP6. The contribution from each specific node in the time profile of marker protein has been dissected separately by considering various terms in the corresponding model equation in [S4 Table](#). Wherever necessary, the inhibitory action related modifications to the relevant rate terms were considered. Inhibitory parameters used are $K_{kib} = 0.0002 \text{ nM}^{-1}$ and $K_{kis} = 0.005 \text{ nM}^{-1}$.

(TIFF)

S1 Table. Ordinary differential equations of the TNF α signaling network and associated algebraic relations.

(PDF)

S2 Table. Description of the entities in the TNF α signaling network model and its state.

(PDF)

S3 Table. Definition of the kinetic parameters involved in the model.

(PDF)

S4 Table. Reaction fluxes affecting the pJNK, pAKT and Caspase3 dynamics.

(PDF)

S5 Table. Branches originating from NF κ B or TNFR1 and ending in the signaling entities pAKT or pJNK.

(PDF)

S6 Table. Coefficients of the fourth order polynomial (Eq S7.1 in S7 Text) under different stimulation conditions.

(PDF)

Acknowledgments

We gratefully acknowledge an access to the IIT Bombay FACS Central Facility and BSBE FACS Facility. SB and BT thank IIT Bombay for their fellowship.

Author Contributions

Conceptualization: Sandip Kar, Ganesh A. Viswanathan.

Data curation: Sharmila Biswas, Baishakhi Tikader.

Formal analysis: Sharmila Biswas, Baishakhi Tikader, Sandip Kar, Ganesh A. Viswanathan.

Funding acquisition: Sandip Kar, Ganesh A. Viswanathan.

Investigation: Sharmila Biswas, Baishakhi Tikader, Sandip Kar, Ganesh A. Viswanathan.

Methodology: Sharmila Biswas, Baishakhi Tikader, Sandip Kar, Ganesh A. Viswanathan.

Project administration: Sandip Kar, Ganesh A. Viswanathan.

Resources: Sharmila Biswas, Baishakhi Tikader, Sandip Kar, Ganesh A. Viswanathan.

Software: Sharmila Biswas, Baishakhi Tikader.

Supervision: Sandip Kar, Ganesh A. Viswanathan.

Validation: Sharmila Biswas, Baishakhi Tikader, Sandip Kar, Ganesh A. Viswanathan.

Visualization: Sharmila Biswas, Baishakhi Tikader, Sandip Kar, Ganesh A. Viswanathan.

Writing – original draft: Sharmila Biswas, Baishakhi Tikader.

Writing – review & editing: Sandip Kar, Ganesh A. Viswanathan.

References

1. Sankar G, Michael K. Missing pieces in the NF κ B puzzle. *Cell*. 2002; 109: S81–96. [https://doi.org/10.1016/s0092-8674\(02\)00703-1](https://doi.org/10.1016/s0092-8674(02)00703-1) PMID: 11983155.
2. Aggarwal BB. Signalling pathways of the TNF superfamily: a double-edged sword. *Nat Rev Immunol*. 2003; 3: 745–756. <https://doi.org/10.1038/nri1184> PMID: 12949498.
3. Hoffmann A, Baltimore D. Circuitry of nuclear factor κ B signaling. *Immunol Rev*. 2006; 210: 171–186. <https://doi.org/10.1111/j.0105-2896.2006.00375.x> PMID: 16623771.
4. Zelová H, Hošek J. TNF- α signalling and inflammation: interactions between old acquaintances. *Inflamm Res*. 2013; 62: 641–651. <https://doi.org/10.1007/s00011-013-0633-0> Epub 2013 May 18. PMID: 23685857.

5. Wallach D, Varfolomeev EE, Malinin NL, Goltsev Y V, Kovalenko A V, Boldin MP. Tumor necrosis factor receptor and Fas signaling mechanisms. *Annu Rev Immunol*. 1999; 17: 331–367. <https://doi.org/10.1146/annurev.immunol.17.1.331> PMID: 10358762.
6. Locksley RM, Killeen N, Lenardo MJ. The TNF and TNF receptor superfamilies: integrating mammalian biology. *Cell*. 2001; 104: 487–501. [https://doi.org/10.1016/s0092-8674\(01\)00237-9](https://doi.org/10.1016/s0092-8674(01)00237-9) PMID: 11239407.
7. Micheau O, Tschopp J. Induction of TNF receptor I-mediated apoptosis via two sequential signaling complexes. *Cell*. 2003; 114: 181–190. [https://doi.org/10.1016/s0092-8674\(03\)00521-x](https://doi.org/10.1016/s0092-8674(03)00521-x) PMID: 12887920.
8. Mantovani A, Allavena P, Sica A, Balkwill F. Cancer-related inflammation. *Nature*. 2008; 454: 436–444. <https://doi.org/10.1038/nature07205> PMID: 18650914.
9. Newton K, Dixit VM. Signaling in innate immunity and inflammation. *Cold Spring Harb Perspect Biol*. 2012; 4: a006049. <https://doi.org/10.1101/cshperspect.a006049> PMID: 22296764; PMCID: PMC3282411.
10. Aggarwal BB, Gupta SC, Kim JH. Historical perspectives on tumor necrosis factor and its superfamily: 25 years later, a golden journey. *Blood, J Am Soc Hematol*. 2012; 119: 651–665. <https://doi.org/10.1182/blood-2011-04-325225> Epub 2011 Nov 3. PMID: 22053109; PMCID: PMC3265196.
11. Shishodia S, Aggarwal BB. Nuclear factor- κ B activation: a question of life or death. *BMB Rep*. 2002; 35: 28–40. <https://doi.org/10.5483/bmbrep.2002.35.1.028> PMID: 16248967.
12. Lopez J, Tait SWG. Mitochondrial apoptosis: killing cancer using the enemy within. *Br J Cancer*. 2015; 112: 957–962. <https://doi.org/10.1038/bjc.2015.85> PMID: 25742467; PMCID: PMC4366906.
13. Jarosz-Griffiths HH, Holbrook J, Lara-Reyna S, McDermott MF. TNF receptor signalling in autoinflammatory diseases. *Int Immunol*. 2019; 31: 639–648. <https://doi.org/10.1093/intimm/dxz024> PMID: 30838383.
14. Sherekar S, Viswanathan GA. Boolean dynamic modeling of cancer signaling networks: Prognosis, progression, and therapeutics. *Comput Syst Oncol*. 2021; 1: e1017. <https://doi.org/10.1002/cso2.1017>
15. Kaufman DR, Choi Y. Signaling by tumor necrosis factor receptors: pathways, paradigms and targets for therapeutic modulation. *Int Rev Immunol*. 1999; 18: 405–427. <https://doi.org/10.3109/08830189909088491> PMID: 10626251.
16. Vilcek J. First demonstration of the role of TNF in the pathogenesis of disease. *J Immunol*. 2008; 181: 5–6. doi: <https://doi.org/10.4049/jimmunol.181.1.5> PMID: 18566362.
17. Fouad YA, Aanei C. Revisiting the hallmarks of cancer. *Am J Cancer Res*. 2017; 7: 1016. PMID: 28560055; PMCID: PMC5446472.
18. Hanahan D, Weinberg RA. The hallmarks of cancer. *Cell*. 2000; 100: 57–70. [https://doi.org/10.1016/s0092-8674\(00\)81683-9](https://doi.org/10.1016/s0092-8674(00)81683-9) PMID: 10647931.
19. Kist M, Vucic D. Cell death pathways: intricate connections and disease implications. *EMBO J*. 2021; 40: e106700. <https://doi.org/10.15252/embj.2020106700> Epub 2021 Jan 13. PMID: 33439509; PMCID: PMC7917554.
20. Janes KA, Albeck JG, Gaudet S, Sorger PK, Lauffenburger DA, Yaffe MB. A systems model of signaling identifies a molecular basis set for cytokine-induced apoptosis. *Science*. 2005; 310: 1646–1653. <https://doi.org/10.1126/science.1116598> PMID: 16339439.
21. Reed JC, Miyashita T, Takayama S, Wang H-G, Sato T, Krajewski S, et al. Bcl-2 family proteins: regulators of cell death involved in the pathogenesis of cancer and resistance to therapy. *J Cell Biochem*. 1996; 60: 23–32. [https://doi.org/10.1002/\(SICI\)1097-4644\(19960101\)60:1%3C23::AID-JCB5%3E3.0.CO;2-5](https://doi.org/10.1002/(SICI)1097-4644(19960101)60:1%3C23::AID-JCB5%3E3.0.CO;2-5) PMID: 8825412.
22. Wajant H, Pfizenmaier K, Scheurich P. Tumor necrosis factor signaling. *Cell Death & Differ*. 2003; 10: 45–65. <https://doi.org/10.1038/sj.cdd.4401189> PMID: 12655295.
23. Van Antwerp DJ, Martin SJ, Kafri T, Green DR, Verma IM. Suppression of TNF α induced apoptosis by NF- κ B. *Science*. 1996; 274: 787–789. <https://doi.org/10.1126/science.274.5288.787> PMID: 8864120
24. Werner SL, Kearns JD, Zadorozhnaya V, Lynch C, O’Dea E, Boldin MP, et al. Encoding NF- κ B temporal control in response to TNF: distinct roles for the negative regulators I κ B α and A20. *Genes & Dev*. 2008; 22: 2093–2101 <https://doi.org/10.1101/gad.1680708> PMID: 18676814
25. Liu Y, Zhou L-J, Wang J, Li D, Ren W-J, Peng J, et al. TNF- α differentially regulates synaptic plasticity in the hippocampus and spinal cord by microglia-dependent mechanisms after peripheral nerve injury. *J Neurosci*. 2017; 37: 871–881. <https://doi.org/10.1523/JNEUROSCI.2235-16.2016> PMID: 28123022
26. Charles KA, Kulbe H, Soper R, Escorcio-Correia M, Lawrence T, Schulteis A, et al. The tumor-promoting actions of TNF- α involve TNFR1 and IL-17 in ovarian cancer in mice and humans. *J Clin Invest*. 2009; 119: 3011–3023. <https://doi.org/10.1172/JCI39065> PMID: 19741298

27. Meyer R, DAlessandro LA, Kar S, Kramer B, She B, Kaschek D, et al. Heterogeneous kinetics of AKT signaling in individual cells are accounted for by variable protein concentration. *Front Physiol.* 2012; 3: 451 <https://doi.org/10.3389/fphys.2012.00451> PMID: 23226133
28. Burow ME, Weldon CB, Collins-Burow BM, Ramsey N, McKee A, Klippel A, et al. Cross-talk between phosphatidylinositol 3-kinase and sphingomyelinase pathways as a mechanism for cell survival/death decisions. *J Biol Chem.* 2000; 275: 9628–9635. <https://doi.org/10.1074/jbc.275.13.9628> PMID: 10734114
29. Vivanco I, Sawyers CL. The phosphatidylinositol 3-kinase—AKT pathway in human cancer. *Nat Rev Cancer.* 2002; 2: 489–501 <https://doi.org/10.1038/nrc839> PMID: 12094235
30. Kandel ES, Skeen J, Majewski N, Di Cristofano A, Pandolfi PP, Feliciano CS, et al. Activation of Akt/protein kinase B overcomes a G2/M cell cycle checkpoint induced by DNA damage. *Mol Cell Biol.* 2002; 22: 7831–7841 <https://doi.org/10.1128/MCB.22.22.7831-7841.2002> PMID: 12391152
31. Gerondakis S, Grossmann M, Nakamura Y, Pohl T, Grumont R. Genetic approaches in mice to understand Rel/NF- κ B and I κ B function: transgenics and knockouts. *Oncogene.* 1999; 18: 6888–6895.
32. Meffert MK, Chang JM, Wiltgen BJ, Fanselow MS, Baltimore D. NF- κ B functions in synaptic signaling and behavior. *Nat Neurosci.* 2003; 6: 1072–1078 <https://doi.org/10.1038/nn1110> PMID: 12947408
33. Behar M, Hoffmann A. Understanding the temporal codes of intra-cellular signals. *Curr Opin Genet & Dev.* 2010; 20: 684–693 <https://doi.org/10.1016/j.gde.2010.09.007> PMID: 20956081
34. Purvis JE, Lahav G. Encoding and decoding cellular information through signaling dynamics. *Cell.* 2013; 152: 945–956 <https://doi.org/10.1016/j.cell.2013.02.005> PMID: 23452846
35. Nurse P. Life, logic and information. *Nature.* 2008; 454: 424–426. <https://doi.org/10.1038/454424a> PMID: 18650911
36. Chen G, Goeddel D V. TNF-R1 signaling: a beautiful pathway. *Science* 80 2002; 296: 1634–1635. <https://doi.org/10.1126/science.1071924> PMID: 12040173.
37. Lau KS, Cortez-Retamozo V, Philips SR, Pittet MJ, Lauffenburger DA, Haigis KM. Multi-scale in vivo systems analysis reveals the influence of immune cells on TNF- α -induced apoptosis in the intestinal epithelium. 2012. <https://doi.org/10.1371/annotation/60833838-f1b9-4f9c-ae0b-485c4acd09c1>
38. Gierut JJ, Wood LB, Lau KS, Lin Y-J, Genetti C, Samatar AA, et al. Network-level effects of kinase inhibitors modulate TNF- α -induced apoptosis in the intestinal epithelium. *Sci Signal.* 2015; 8: ra129—ra129. <https://doi.org/10.1126/scisignal.aac7235> PMID: 26671150; PMID: PMC4812576
39. Bouwmeester T, Bauch A, Ruffner H, Angrand P-O, Bergamini G, Croughton K, et al. A physical and functional map of the human TNF- α /NF- κ B signal transduction pathway. *Nat Cell Biol.* 2004; 6: 97–105. <https://doi.org/10.1038/ncb1086> Epub 2004 Jan 25. Erratum in: *Nat Cell Biol.* 2004 May;6(5):465. PMID: 14743216.
40. Zhang Q, Gupta S, Schipper DL, Kowalczyk GJ, Mancini AE, Faeder JR, et al. NF- κ B dynamics discriminate between TNF doses in single cells. *Cell Syst.* 2017; 5: 638–645. <https://doi.org/10.1016/j.cels.2017.10.011> Epub 2017 Nov 8. PMID: 29128333; PMID: PMC5746429.
41. Son M, Wang AG, Tu H-L, Metzger MO, Patel P, Husain K, et al. NF- κ B responds to absolute differences in cytokine concentrations. *Sci Signal.* 2021;14. <https://doi.org/10.1126/scisignal.aaz4382> PMID: 34211635; PMID: PMC8244746.
42. Lipniacki T, Puszynski K, Paszek P, Brasier AR, Kimmel M. Single TNF α trimers mediating NF- κ B activation: stochastic robustness of NF- κ B signaling. *BMC Bioinformatics.* 2007; 8: 1–20. <https://doi.org/10.1186/1471-2105-8-376>
43. Schlatter R, Schmich K, Vizcarra IA, Scheurich P, Sauter T, Borner C, et al. ON/OFF and beyond—A Boolean model of apoptosis. *PLoS Comput Biol.* 2009;5. <https://doi.org/10.1371/journal.pcbi.1000595> PMID: 20011108
44. Calzone L, Tournier L, Fourquet S, Thieffry D, Zhivotovsky B, Barillot E, et al. Mathematical modelling of cell-fate decision in response to death receptor engagement. *PLoS Comput Biol.* 2010;6. <https://doi.org/10.1371/journal.pcbi.1000702> PMID: 20221256
45. Matveeva A, Fichtner M, McAllister K, McCann C, Sturrock M, Longley DB, et al. Heterogeneous responses to low level death receptor activation are explained by random molecular assembly of the Caspase-8 activation platform. *PLoS Comput Biol.* 2019; 15: 1–22. <https://doi.org/10.1371/journal.pcbi.1007374> PMID: 31553717
46. Lee REC, Qasaimeh MA, Xia X, Juncker D, Gaudet S. NF- κ B signalling and cell fate decisions in response to a short pulse of tumour necrosis factor. *Sci Rep.* 2016; 6: 1–12. <https://doi.org/10.1038/srep39519>

47. Buchbinder JH, Pischel D, Sundmacher K, Flassig RJ, Lavrik IN. Quantitative single cell analysis uncovers the life/death decision in CD95 network. *PLoS Comput Biol*. 2018; 14: e1006368. <https://doi.org/10.1371/journal.pcbi.1006368> PMID: 30256782
48. Márquez-Jurado S, Díaz-Colunga J, das Neves RP, Martínez-Lorente A, Almázán F, Guantes R, et al. Mitochondrial levels determine variability in cell death by modulating apoptotic gene expression. *Nat Commun*. 2018; 9: 1–11. <https://doi.org/10.1038/s41467-017-02787-4>
49. Lee KY, Chang W, Qiu D, Kao PN, Rosen GD. PG490 (triptolide) cooperates with tumor necrosis factor- α to induce apoptosis in tumor cells. *J Biol Chem*. 1999; 274: 13451–13455. <https://doi.org/10.1074/jbc.274.19.13451> PMID: 10224110.
50. Leaner V, Birrer MJ, Rana A, Shen YH, Godlewski J, Zhu J, et al. Cross-talk between JNK/SAPK and ERK/MAPK pathways: sustained activation of JNK blocks ERK activation by mitogenic factors. *J Biol Chem*. 2003; 278: 26715–26721 <https://doi.org/10.1074/jbc.M303264200> Epub 2003 May 8. PMID: 12738796.
51. Ventura J-J, Hübner A, Zhang C, Flavell RA, Shokat KM, Davis RJ. Chemical genetic analysis of the time course of signal transduction by JNK. *Mol Cell*. 2006; 21: 701–710. <https://doi.org/10.1016/j.molcel.2006.01.018> PMID: 16507367
52. Ozes ON, Akca H, Gustin JA, Mayo LD, Pincheira R, Korgaonkar CK, et al. Tumor Necrosis Factor- α /Receptor Signaling Through the Akt Kinase. *Cell Signaling in Vascular Inflammation*. Springer; 2005. pp. 13–22 <https://doi.org/10.1002/ijc.24748> PMID: 19609947
53. Deng Y, Ren X, Yang L, Lin Y, Wu X. A JNK-dependent pathway is required for TNF α -induced apoptosis. *Cell*. 2003; 115: 61–70 [https://doi.org/10.1016/s0092-8674\(03\)00757-8](https://doi.org/10.1016/s0092-8674(03)00757-8) PMID: 14532003
54. Lamb JA, Ventura J-J, Hess P, Flavell RA, Davis RJ. JunD mediates survival signaling by the JNK signal transduction pathway. *Mol Cell*. 2003; 11: 1479–1489 [https://doi.org/10.1016/s1097-2765\(03\)00203-x](https://doi.org/10.1016/s1097-2765(03)00203-x) PMID: 12820962.
55. Krutzik PO, Nolan GP. Fluorescent cell barcoding in flow cytometry allows high-throughput drug screening and signaling profiling. *Nat Methods*. 2006; 3: 361–368. <https://doi.org/10.1038/nmeth872> PMID: 16628206
56. Manohar S, Shah P, Biswas S, Mukadam A, Joshi M, Viswanathan G. Combining fluorescent cell barcoding and flow cytometry-based phospho-ERK1/2 detection at short time scales in adherent cells. *Cytom Part A*. 2019; 95: 192–200. <https://doi.org/10.1002/cyto.a.23602> Epub 2018 Oct 2. PMID: 30277662.
57. Sawada M, Kiyono T, Nakashima S, Shinoda J, Naganawa T, Hara S, et al. Molecular mechanisms of TNF- α -induced ceramide formation in human glioma cells: p53-mediated oxidant stress-dependent and-independent pathways. *Cell Death & Differ*. 2004; 11: 997–1008. <https://doi.org/10.1038/sj.cdd.4401438>
58. Wicovsky A, Müller N, Daryab N, Marienfeld R, Kneitz C, Kavuri S, et al. Sustained JNK activation in response to tumor necrosis factor is mediated by caspases in a cell type-specific manner. *J Biol Chem*. 2007; 282: 2174–2183 <https://doi.org/10.1074/jbc.M606167200> Epub 2006 Nov 22. PMID: 17121845
59. Aikin R, Maysinger D, Rosenberg L. Cross-talk between phosphatidylinositol 3-kinase/AKT and c-jun NH2-terminal kinase mediates survival of isolated human islets. *Endocrinology*. 2004; 145: 4522–4531 <https://doi.org/10.1210/en.2004-0488> Epub 2004 Jul 8 PMID: 15242986
60. Wullaert A, Heynink K, Beyaert R. Mechanisms of crosstalk between TNF-induced NF- κ B and JNK activation in hepatocytes. *Biochem Pharmacol*. 2006; 72: 1090–1101. <https://doi.org/10.1016/j.bcp.2006.07.003> Epub 2006 Aug 24. PMID: 16934229.
61. Teranishi F, Takahashi N, Gao N, Akamo Y, Takeyama H, Manabe T, et al. Phosphoinositide 3-kinase inhibitor (wortmannin) inhibits pancreatic cancer cell motility and migration induced by hyaluronan in vitro and peritoneal metastasis in vivo. *Cancer Sci*. 2009; 100: 770–777. <https://doi.org/10.1111/j.1349-7006.2009.01084.x> PMID: 19469020.
62. Zhang F, Zhang T, Jiang T, Zhang R, Teng Z, Li C, et al. Wortmannin potentiates roscovitine-induced growth inhibition in human solid tumor cells by repressing PI3K/Akt pathway. *Cancer Lett*. 2009; 286: 232–239 <https://doi.org/10.1016/j.canlet.2009.05.039> Epub 2009 Jun 21 PMID: 19541408
63. Arcaro A, Wymann MP. Wortmannin is a potent phosphatidylinositol 3-kinase inhibitor: the role of phosphatidylinositol 3, 4, 5-trisphosphate in neutrophil responses. *Biochem J*. 1993; 296: 297–301 <https://doi.org/10.1042/bj2960297> PMID: 8257416; PMCID: PMC1137693
64. Ferby IM, Waga I, Sakanaka C, Kume K, Shimizu T. Wortmannin inhibits mitogen-activated protein kinase activation induced by platelet-activating factor in guinea pig neutrophils. *J Biol Chem*. 1994; 269: 30485–30488. [https://doi.org/10.1016/S0021-9258\(18\)43839-2](https://doi.org/10.1016/S0021-9258(18)43839-2) PMID: 7982965
65. Ferby IM, Waga I, Hoshino M, Kume K, Shimizu T. Wortmannin Inhibits Mitogen-activated Protein Kinase Activation by Platelet-activating Factor through a Mechanism Independent of p85/p110-type

- Phosphatidylinositol 3-Kinase (*). *J Biol Chem.* 1996; 271: 11684–11688. <https://doi.org/10.1074/jbc.271.20.11684> PMID: 8662643
66. Manna SK, Aggarwal BB. Wortmannin inhibits activation of nuclear transcription factor NF κ B and activated protein-1 induced by lipopolysaccharide and phorbol ester. *FEBS Letters.* 2000; 473:113–118. [https://doi.org/10.1016/s0014-5793\(00\)01501-5](https://doi.org/10.1016/s0014-5793(00)01501-5) PMID: 10802070
 67. Bennett BL, Sasaki DT, Murray BW, O'Leary EC, Sakata ST, Xu W, et al. SP600125, an anthrapyrazolone inhibitor of Jun N-terminal kinase. *Proc Natl Acad Sci.* 2001; 98: 13681–13686. <https://doi.org/10.1073/pnas.251194298> PMID: 11717429; PMCID: PMC61101.
 68. Moon D-O, Kim M-O, Kang C-H, Lee J-D, Choi YH, Kim G-Y. JNK inhibitor SP600125 promotes the formation of polymerized tubulin, leading to G 2/M phase arrest, endoreduplication, and delayed apoptosis. *Exp & Mol Med.* 2009; 41: 665–677 <https://doi.org/10.3858/emmm.2009.41.9.073> PMID: 19478553
 69. Brandt B, Abou-Eladab EF, Tiedge M, Walzel H. Role of the JNK/c-Jun/AP-1 signaling pathway in galectin-1-induced T-cell death. *Cell death & Dis.* 2010; 1: e23 <https://doi.org/10.1038/cddis.2010.1> PMID: 21364631; PMCID: PMC3032336.
 70. Shaulian E, Karin M. AP-1 as a regulator of cell life and death. *Nat Cell Biol.* 2002; 4: E131–E136. <https://doi.org/10.1038/ncb0502-e131> PMID: 11988758
 71. Eferl R, Wagner EF. AP-1: A double-edged sword in tumorigenesis. *Nat Rev Cancer.* 2003; 3: 859–868 <https://doi.org/10.1038/nrc1209> PMID: 14668816
 72. Mezosi E, Wang SH, Utsugi S, Bajnok L, Bretz JD, Gauger PG, et al. Induction and regulation of fas-mediated apoptosis in human thyroid epithelial cells. *Mol Endocrinol.* 2005; 19: 804–811 <https://doi.org/10.1210/me.2004-0286> PMID: 15563545
 73. Abreu-Martin MT, Palladino AA, Faris M, Carramanzana NM, Nel AE, Targan SR. Fas activates the JNK pathway in human colonic epithelial cells: Lack of a direct role in apoptosis. *Am J Physiol—Gastrointest Liver Physiol.* 1999; 276: 599–605. <https://doi.org/10.1152/ajpgi.1999.276.3.G599> PMID: 10070035
 74. Lear RA. The Root Cause in the dramatic rise of Chronic Disease. *Res Sept.* 2016.
 75. Liu Y, Imlay JA. Cell death from antibiotics without the involvement of reactive oxygen species. *Science* 80. 2013; 339: 1210–1213. <https://doi.org/10.1126/science.1232751> PMID: 23471409; PMCID: PMC3731989.
 76. Rehm M, Huber HJ, Dussmann H, Prehn JHM. Systems analysis of effector caspase activation and its control by X-linked inhibitor of apoptosis protein. *EMBO J.* 2006; 25: 4338–4349. <https://doi.org/10.1038/sj.emboj.7601295> Epub 2006 Aug 24 PMID: 16932741; PMCID: PMC1570423
 77. Zhang X-P, Liu F, Wang W. Two-phase dynamics of p53 in the DNA damage response. *PNAS.* 2011; 108:8990–8995. <https://doi.org/10.1073/pnas.1100600108> PMID: 21576488.
 78. Zhang X-P, Liu F, Cheng Z, Wang W. Cell fate decision mediated by p53 pulses. *PNAS.* 2009; 106:12245–12250. <https://doi.org/10.1073/pnas.0813088106> PMID: 19617533.
 79. Chen S-h, Forrester W, Lahav G. Schedule-dependent interaction between anticancer treatments. *Science.* 2016; 351:1204–1208. <https://doi.org/10.1126/science.aac5610> PMID: 26965628.
 80. Wu M, Ye H, Tang Z, et al. p53 dynamics orchestrates with binding affinity to target genes for cell fate decision. *Cell Death and Disease.* 2017; 9:e3130. <https://doi.org/10.1038/cddis.2017.492> PMID: 29048401.
 81. Koh G, Lee D-Y. Mathematical modeling and sensitivity analysis of the integrated TNF α -mediated apoptotic pathway for identifying key regulators. *Comput Biol Med.* 2011; 41: 512–528. <https://doi.org/10.1016/j.combiomed.2011.04.017> Epub 2011 May 31 PMID: 21632045
 82. Schliemann M, Bullinger E, Borchers S, Allgöwer F, Findeisen R, Scheurich P. Heterogeneity reduces sensitivity of cell death for TNF-stimuli. *BMC Syst Biol.* 2011; 5: 1–11. <https://doi.org/10.1186/1752-0509-5-204>
 83. Ussat S, Werner U-E, Kruse M-L, Lüschen S, Scherer G, Kabelitz D, et al. Upregulation of p21WAF1/Cip1 precedes tumor necrosis factor-induced necrosis-like cell death. *Biochem Biophys Res Commun.* 2002; 294: 672–679 [https://doi.org/10.1016/S0006-291X\(02\)00532-6](https://doi.org/10.1016/S0006-291X(02)00532-6) PMID: 12056822
 84. Spencer SL, Gaudet S, Albeck JG, Burke JM, Sorger PK. Non-genetic origins of cell-to-cell variability in TRAIL-induced apoptosis. *Nature.* 2009; 459: 428–432. <https://doi.org/10.1038/nature08012> Epub 2009 Apr 12. PMID: 19363473; PMCID: PMC2858974.
 85. Maiwald T, Timmer J. Dynamical modeling and multi-experiment fitting with PottersWheel. *Bioinformatics.* 2008; 24: 2037–2043. <https://doi.org/10.1093/bioinformatics/btn350> Epub 2008 Jul 9. PMID: 18614583; PMCID: PMC2530888.
 86. Ritz C, Streibig JC. Bioassay analysis using R. *J Stat Softw.* 2005; 12: 1–22. <https://doi.org/10.18637/jss.v012.i05>